Integrated Optics Components and Devices Using Periodic Structures

TOSHIAKI SUHARA AND HIROSHI NISHIHARA, MEMBER, IEEE

(*Invited Paper*)

Abstract—**The selected research activities on integrated optics components and devices using periodic structures are reviewed, with emphasis on the authors' works employing the electron-beam writing technique. The periodic structures include static gratings and dynamic ones produced through acoustooptic (AO) and electrooptic (EO) effects. They provide a variety of passive functions and effective means for guided-wave control. The review is made from the integration point of view, including the most recent results. First, the theoretical fundamentals are outlined and the electron-beam writing techniques, including the writing system, are discussed. Next, passive components (grating deflectors, filters, lenses, couplers, etc.) and elements for guided-wave controlling and detecting (AO and EO grating elements and photodetectors) are described. Then, integrated optic devices, i.e., wavelength demultiplexers, RF spectrum analyzers, optical disk pickup, etc., are presented. Finally, the possibility of future applications is discussed.**

I. INTRODUCTION

SINCE the earliest stage of integrated optics research, periodic structures in waveguides have been of great interest [1]–[5]. The periodic structures for integrated optics include not only passive (static) optical gratings, but also dynamic (controllable) ones which are produced through acoustooptic or electrooptic effects by applying electric signals to periodic electrodes.

The importance of the periodic structures or gratings results from the variety of functions they can perform.

1) Phase Matching and Wave Coupling: The phase matching function of gratings gives rise to various couplings of two (or more) waves satisfying the matching condition. Therefore, gratings can serve as input/output couplers, waveguide interfaces, deflectors, reflectors, mode/polarization convertors, and mode/polarization filters, etc.

2) Wavefront Conversion: Modulated gratings perform various complex wavefront conversions based upon the principle of holography. A typical example is the lens functions. Two or more functions, e.g., deflection, splitting and focusing, can be fused into a wavefront conversion; they can be realized by a single grating component.

3) Wavelength Dispersion: Gratings are typically elements of high wavelength dispersion; functions 1) and 2) are wavelength dependent. This enables their application to wavelength filters, separators/combiners, and multi-/demultiplexers.

Thus, gratings provide many of the passive functions, and the dynamic gratings can be an effective means for guided-wave control.

Recent research and development activities in integrated optics have been directed to the implementation of fully integrated, complex devices incorporating several functions to perform a specific operation. Also, from the integration point of view, the periodic structures offer many advantages.

1) Planar Structure: The gratings have a planar structure within a thin layer. This implies they can be fabricated by the well-established planar microfabrication processes, i.e., photo and electron-beam lithographies. They are mass-producible with excellent accuracy and reproducibility.

2) Many Functions: The many and complex functions realizable with gratings of the same or similar structure minimize the number of components and the fabrication process. Several kinds of grating components can possibly be fabricated simultaneously.

3) Redundancy: The characteristics of periodic elements are insensitive to point (and line) defects. This assures good yield, even in complex integrated devices.

Along with the versatility and the integration compatibilities, applications of periodic structures are an attractive subarea of increasing importance.

In this paper, the authors would like to review the current status of technology in the subarea of integrated optics using periodic structures, especially from the integration point of view. The emphasis is on the authors' work employing the electron-beam writing technique. Some of the most recent results and discussions of future works are also included. At first, the theoretical fundamentals required for the analysis and design of gratings for integrated optics are outlined in Section II. Then, Section III presents the fabrication techniques based upon electron-beam writing including the writing system construction. Section IV describes the passive components. Section V presents elements for guided-wave controlling and detecting, i.e., acoustooptic and electrooptic grating elements and integrated photodetectors. Section VI presents

Manuscript received November 12, 1985; revised February 13, 1986. This work was supported by a series of Scientific Research Grant-in-Aids from the Ministry of Education, Science, and Culture of Japan.

The authors are with the Department of Electronics, Faculty of Engineering, Osaka University, 2-1, Yamada-Oka, Suita, Osaka 565, Japan.

IEEE Log Number 8608183.

0018-9197/86/0600-0845$01.00 © 1986 IEEE

integrated optic devices, i.e., wavelength demultiplexers, RF spectrum analyzers, an optical disk pickup, and an optical printer head, etc., which are constructed by integrating elements described in Sections IV and V. And finally, Section VII discusses the possibilities of future applications in selected fields.

II. Fundamentals

Since there are many review articles dealing with theoretical analysis and the design of grating components for integrated optics [4]–[7], only the fundamental concepts and formulas required in the following sections will be outlined here.

A. Waveguide Grating Descriptions

Fig. 1 shows various grating structures in a waveguide. They can be classified into the index modulation type and the relief type. In either case, the grating can be described by the change in the (relative) dielectric permittivity $\Delta\epsilon$ caused by the grating in the fundamental waveguide structure. Being a periodic function, $\Delta\epsilon$ can be written in Fourier series as

$$\Delta\epsilon(x, y, z) = \sum_q \Delta\epsilon_q(x) \exp(-jq\boldsymbol{K} \cdot \boldsymbol{r}) \qquad (1)$$

in the grating layer and $\Delta\epsilon = 0$ outside the layer. The grating vector $\boldsymbol{K}$ is in the plane of waveguide (yz plane), and the magnitude is correlated with the period Λ by $|\boldsymbol{K}| = K = 2\pi/\Lambda$. Equation (1) can be used not only for the index modulation type [Fig. 1(a)], but also for the relief type [Fig. 1(b)]. The relief can be described by a binary permittivity modulation $\Delta\epsilon(x, y, z)$ taking the values for the relief material and the air, and $\Delta\epsilon(x, y, z)$ is written in Fourier series with the coefficient $\Delta\epsilon_q(x)$ dependent only on x.

B. Coplanar Coupling Between Guided Waves

In a planar waveguide, guided waves can propagate in arbitrary directions along the plane of the waveguide. A grating in such a structure couples guided waves, of the same or different modes, propagating in different directions. The coplanar coupling is of great importance because of the many functions, e.g., guided-wave deflection, reflection, mode and polarization conversion, mode and wavelength filtering.

The phase-matching condition, i.e., the Bragg condition, for the coupling between two guided waves having propagation vectors $\boldsymbol{\beta}_i$ and $\boldsymbol{\beta}_d$, respectively, is given by

$$\boldsymbol{\beta}_d = \boldsymbol{\beta}_i + q\boldsymbol{K} (q = \pm 1, \pm 2, \cdots) \qquad (2)$$

where q is the order of diffraction. The vector $\boldsymbol{\beta}$ has the magnitude $|\boldsymbol{\beta}| = \beta$, which is correlated with the wavelength in free space λ and the mode index n_e by $\beta = 2\pi n_e/\lambda$.

An important parameter related to the thickness L of the grating is Q defined by

$$Q = K^2 L/\beta. \qquad (3)$$

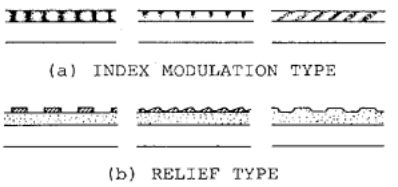

Fig. 1. Various grating structures for integrated optics.

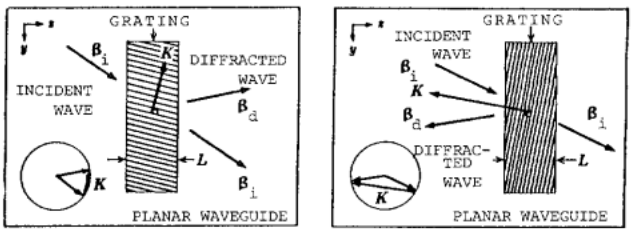

Fig. 2. Coplanar coupling of guided waves by a grating.

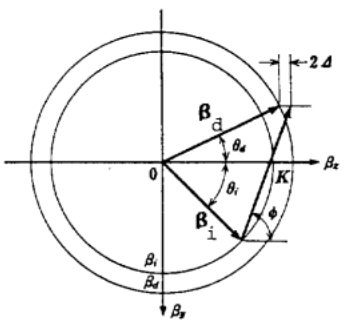

Fig. 3. Wave vector diagram of coplanar coupling.

The parameter is used to classify the coplanar coupling into two categories. When $Q \lesssim 1$, the coupling is the Raman–Nath diffraction which is characterized by the generation of many diffraction orders and a relatively low efficiency; the details will not be discussed here. When $Q \gtrsim 10$ (''thick'' grating), on the other hand, the coupling is the Bragg diffraction which allows high diffraction efficiency into one order.

Fig. 2 shows the coplanar Bragg grating configurations. The wave vector diagram near the Bragg condition (2) is depicted in Fig. 3. The Bragg condition (2) can be rewritten as

$$\cos(\theta_{iB} - \phi) = -(\beta_i^2 + q^2K^2 - \beta_d^2)/2\beta_i qK \qquad (4)$$

where θ_{iB} is the (qth order) Bragg incident angle. Assuming

$$\Delta\theta_i = \theta_i - \theta_{iB}, \ \Delta\lambda = \lambda' - \lambda \qquad (5)$$

are deviations in angle and wavelength, respectively, from the Bragg condition, the phase mismatch 2Δ (Fig. 3) can be written as

$$2\Delta = -[qK\beta_i \sin(\phi - \theta_{iB})/\beta_d \cos\theta_{dB}]\Delta\theta_i \qquad (6)$$

$$2\Delta = -[qK \cos(\theta_{dB} - \phi)/\cos\theta_{dB}](\Delta\lambda/\lambda). \qquad (7)$$

The characteristics of Bragg gratings have been analyzed by the coupled-wave theory [8], [9].

1) Transmission-Type Coupling: The diffraction effi-

ciency is given by

$$\eta = \sin^2 (\nu^2 + \xi^2)^{1/2}/(1 + \xi^2/\nu^2) \quad (8)$$

$$\nu = \kappa L/\sqrt{\cos \theta_i \cos \theta_d}, \qquad \xi = \Delta \cdot L \quad (9)$$

where κ is the coupling coefficient. Under the Bragg condition ($2\Delta = 0$), (8) reduces to

$$\eta_0 = \sin^2 \nu = \sin^2 (\kappa L/\sqrt{\cos \theta_i \cos \theta_d}) \quad (10)$$

and shows that the efficiency is a periodic function of ν and 100 percent efficiency is obtained when $\nu = \pi/2$.

2) Reflection-Type Coupling: The diffraction efficiency is given by

$$\eta = [1 + (1 - \xi^2/\nu^2)/\sinh^2 (\nu - \xi^2)^{1/2}]^{-1} \quad (11)$$

$$\nu = \kappa L/\sqrt{\cos \theta_i |\cos \theta_d|}, \qquad \xi = \Delta \cdot L. \quad (12)$$

Under the Bragg condition ($2\Delta = 0$), (11) reduces to

$$\eta_0 = \tanh^2 \nu = \tanh^2 (\kappa L/\sqrt{\cos \theta_i |\cos \theta_d|}) \quad (13)$$

and shows that the efficiency is a monotonic increasing function of ν giving $\eta \geqq 84.1$ percent for $\nu \geqq \pi/2$.

The Bragg gratings exhibit angular and wavelength selectivities, i.e., the reduction of efficiency due to the deviation from the Bragg condition. The selectivities can be evaluated by combining (5)–(7) with (8) and (9) or (11) and (12). The coupling coefficient κ can be calculated by making a overlap integral of $\Delta\epsilon_q(x)$ in (1) with the relevant guided mode field profiles [9], [10].

The above-described coplanar couplings include, as a special case, the collinear couplings where the propagation vectors of the relevant waves are parallel to each other. Such collinear grating configurations can be used with channel waveguide(s) structure as well as with planar waveguide.

Although this paper does not include a review of active integrated optics devices, it should be mentioned that one of the most important current applications of periodic structures is distributed feedback (DFB) and distributed Bragg reflection (DBR) lasers [4], [11], [12], which use the collinear contradirectional coupling for the reflector function.

C. Coupling Between Guided and Radiation Waves

Fig. 4 illustrates the coupling between a guided wave and radiation waves. When a guided wave enters the grating region, the grating (the vector parallel to the guided-beam propagation) yields spatial harmonics with propagation constants

$$\beta_q = \beta_0 + qK \qquad (q = 0, \pm 1, \pm 2, \cdots),$$

$$\beta_0 \simeq \beta. \quad (14)$$

If orders q which satisfy $|\beta_q| < n_c k$ or $|\beta_q| < n_s k$ are present, the harmonics radiate into the air and/or the substrate with the angle θ_q^c and θ_q^s given by

$$n_c k \sin \theta_q^c = n_s k \sin \theta_q^s = \beta_q = n_e k + qK, \quad (15)$$

respectively. Whereas Fig. 4(a) and (b) shows the multi-beam and two-beam couplings, respectively, with the first-order radiation into both air and substrate, a larger grating period results in multibeam coupling with first-order substrate radiation. The guided wave leaks through radiation due to the distributed coupling; the guided wave amplitude decays exponentially.

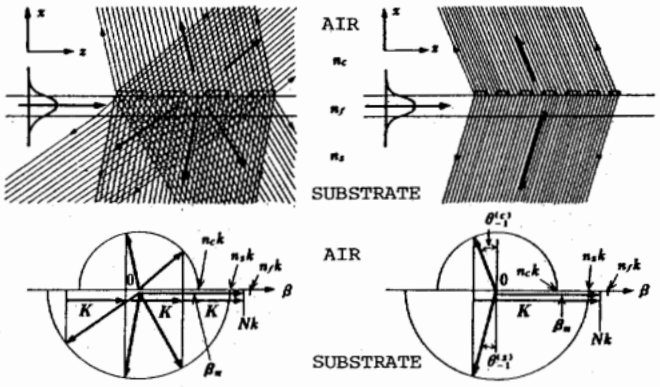

Fig. 4. Coupling between guided wave and radiation wave by a grating.

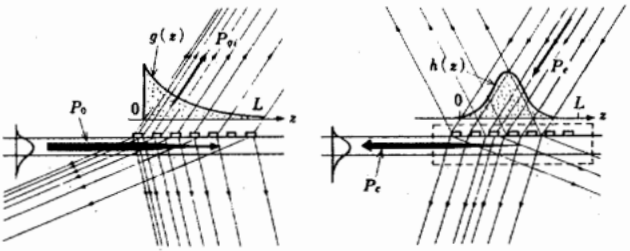

Fig. 5. Input and output coupling by a grating.

Fig. 5 illustrates the input and output couplings. The output coupling efficiency of a grating coupler having a length L can be written as

$$\eta^i_{q(\text{out})} = P^i_q[1 - \exp(-2\alpha_r L)] \quad (16)$$

for the qth order (i) radiation, where $i(=c$ or $s)$ distinguishes air and substrate. Here α_r denotes the radiation decay factor and P^i_q (equal to the efficiency for $L = \infty$) is the fractional power to $q - i$ radiation. The output beam has the exponential profile $g(z)$ as shown in Fig. 5(a). The input coupling efficiency, on the other hand, can be written [13] as

$$\eta^i_{q(\text{in})} = P^i_q I(g, h); \quad (17)$$

$$I(g, h) = \left[\int_0^L gh\, dz\right]^2 \Big/ \left[\int_{-\infty}^{\infty} g^2\, dz \int_{-\infty}^{\infty} h^2\, dz\right] \quad (18)$$

for a $q - i$ input having a profile $h(z)$ as shown in Fig. 5(b). The overlap integral $I(g, h)$ is unity when h resembles g, and otherwise is smaller than unity [14].

It is important for design purpose to correlate the radiation decay factor α_r and the fractional power P^i_q with the device parameters. The required calculations can be made by rigorous space-harmonics expansion based upon Floquet's theorem [15], coupled wave analysis [16], and perturbation analyses [17]–[19].

D. Wavefront Conversions

While the above discussions were with uniform gratings, the principle of holography [20] indicates that various wavefront conversion functions are added by spatially modulating the grating. Such conversion can be incorporated with both guided-to-guided and guided-to-radiation coupling. Suppose that Φ_i and Φ_o are the phase distribution functions of the input wavefront and the desired output wavefront, respectively; then the difference in the grating plane can be written as

$$\Delta\Phi(y, z) = \Phi_o(y, z) - \Phi_i(y, z). \tag{19}$$

The desired wavefront conversion is accomplished by giving a phase modulation equal to $\Delta\Phi$ to the input wavefront. The grating (hologram) for such phase modulation consists of grating lines described by

$$\Delta\Phi(y, z) = 2m\pi \quad (m = \cdots, -2, -1, 0, +1, +2, \cdots). \tag{20}$$

The grating can be obtained by recording the interference between the two wavefronts just as hologram recording. However, it should be noted that, except for the conversion between plane wavefronts, the use of a wavelength different from that used in fabrication results in an aberration since the phase functions are wavelength dependent [(19) includes a $2\pi/\lambda$ factor].

III. Electron-Beam Writing Techniques

A. EB Writing Technique Versus Holographic Lithography

The well-established fabrication technique for integrated optics gratings is holographic interference lithography [21]. The technique has been widely used because of the following advantages: 1) fabrication of small-period gratings with simple apparatus, 2) good period controllability and high period uniformity, and 3) easy fabrication of large-area gratings. However, the drawbacks 1) small flexibility in fabricating modulated gratings, 2) setup rearrangements required for parameter changes, and 3) possible noise problem and difficult definition of grating area (caused by spurious diffraction and interference) may limit the applications.

Another important technique discussed here is computer-controlled electron-beam (EB) writing. Grating patterns, generated by computation using mathematical formulas, are written by focused EB scanning. Therefore, the EB writing is inherently free from the drawbacks of the interference method. The technique provides potential advantages including 1) very high resolution, 2) large flexibility in fabricating modulated gratings, 3) easy parameter changes, and 4) fabrication of low-noise gratings with a well-defined frame at accurately assigned position and orientation. The merit 2) is especially important in fabricating gratings having a (complex) wavefront conversion function such as grating lenses where the interference method results in difficulty, i.e., serious aberration problems caused by the wavelength difference between light for the fabrication and the use. The merits 3) and 4) match the technque to the integration of various grating components. Although the EB technique is rather inferior in the period uniformity and fine control as compared to the interference method and has limited writing area, it is acceptable in many integrated optics applications. Thus, the EB technique has features almost complementary to those of the interference technique, and therefore can greatly extend the applications of periodic structures.

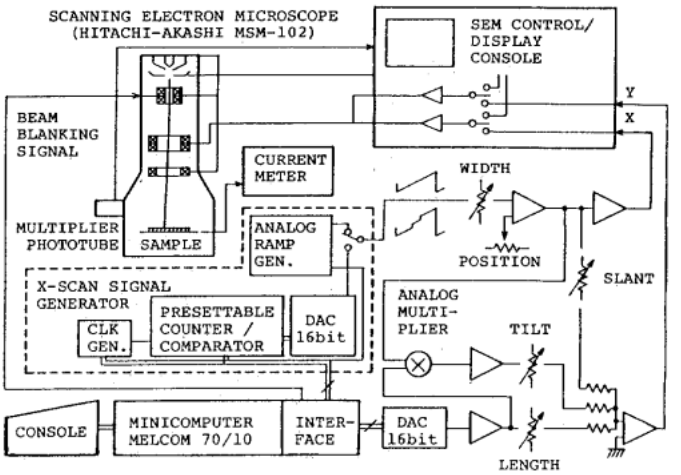

Fig. 6. Block diagram of an electron-beam writing system designed for optical component fabrication.

B. EB Writing System

Computer-controlled EB writing systems have been developed for the semiconductor IC industry and are commercially available. Being of general purpose, they also can be employed for integrated optics fabrication. However, for the fabrication of optical components, different requirements exist; in many cases, it is required to write smooth lines with curvature and/or inclination, and a continuous change in parameters may be involved. For this reason, it is more convenient and effective to have a special system. Such a system has been developed and is being used in the authors' laboratory. The system consists of an ordinary scanning electron microscope (SEM) (Hitachi-Akashi MSM-102) and a specially designed scanning controller connected to a minicomputer (MELCOM 70/10). The design philosophy is that 1) analog signal processing should be incorporated with digital control by the computer to meet the above requirements, and 2) hardware units for specialized scanning modes should be built in the controller to relieve the software dependence and have high-speed operation.

The block diagram of the system is shown in Fig. 6; the system has the following functions.

**EB Blanking:* The EB blanking signal is applied to the condenser lens circuit instead of to independent electrodes. This quasi blanking, being of slow speed, is used only at the beginning and the end of a writing. The un-

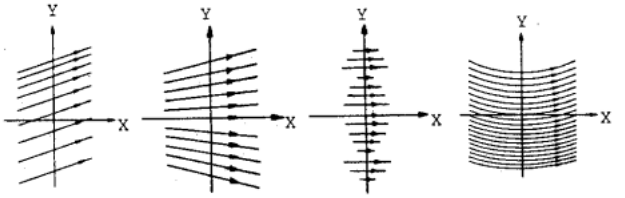

Fig. 7. Schematic illustrations of the scanning modes of the electron-beam writing system shown in Fig. 6.

necessary EB exposure during a writing is avoided by rapid jumps of EB position.

**Y Scan:* The *Y* position of the EB is assigned by a 16 bit DAC. An active filter is inserted to tailor the time constant for the scanning line smoothing. In writing gratings, this *Y* direction is usually taken along the period direction; uniform and arbitrarily chirped periodic patterns can be written by taking advantage of full flexibility of the software control.

**X-Scan A:* The analog ramp generator assures writing of exteremely smooth straight lines with constant length and speed.

**X-Scan B:* The digital ramp generator consisting of a clock generator, presettable counter/comparator, and 16 bit DAC enables writing of line segments with variable length and position; the starting and ending points can be computer controlled. Inhibiting the clock results in the ordinary digital *X-Y* address operation. The clock synchronization to the *Y*-data strobe enables the curved-line scanning with automatic *X* scanning.

**Variable Clock:* The clock frequency can be changed on any occasion by computer control to enable the variable speed scanning for gradient-dose writing and/or line width control.

**Slant:* Analog adding of *X* and *Y* signals enables slanted line scanning at constant inclination angle.

**Tilt:* Analog multiplying of *X* and *Y* signals added to the *Y* signal enables variable-tilt line scanning with the inclination proportional to the *Y* coordinate.

**Analog Adjustments:* Writing parameters such as relative width, length, slant, tilt, position, and speeds can be adjusted by analog potentiometers in addition to the software control.

Fig. 7 illustrates the typical EB writing modes. The system has actually been used for fabrication of the devices reviewed in the following sections; all the patterns were written within 3–30 min., including the computation time.

C. EB Writing Techniques

1) EB Lithography with Resist: In ordinary EB lithography, patterns are written in an EB resist. As shown in Fig. 8, periodic patterns can be written by (a) the painting-out method, (b) the line-drawing method, or (c) the gradient-dose method; (a) and (b) are suitable for gratings of large and small periods, respectively, and (c) enables fabrication of gradient-thickness cross section, e.g., blazed gratings [22]. If the substrate (waveguide) is an insulator, a very thin (~ 100 Å) conductive (Au, Al, etc.)

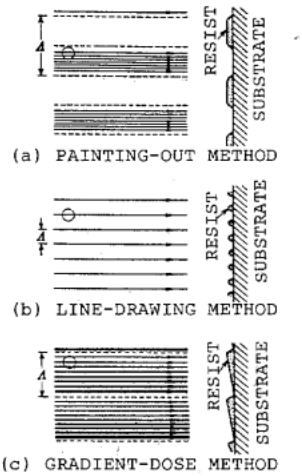

Fig. 8. Electron-beam scanning methods for writing gratings.

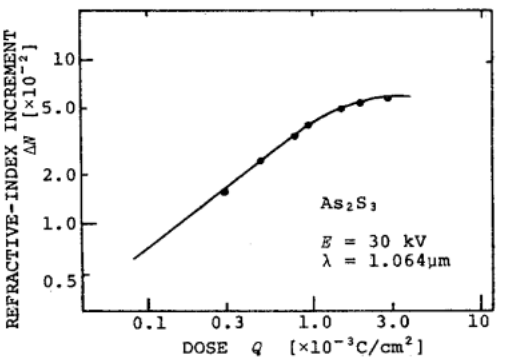

Fig. 9. Dependence of the refractive index change of chalcogenide film upon electron-beam dose [42].

layer must be deposited to avoid the charging-up problem during the writing, and the coating must be removed before the development. The use of an SiO_2/Si waveguide substrate eliminates the need for this process.

In some cases, the resist pattern itself can be used as a grating. More generally, the pattern is transferred to waveguide, cladding, or hard-mask layers by the liftoff and/or etching techniques [21]. And after additional etching or diffusion process using the hard mask, if necessary, the final structure is obtained.

2) Resistless EB Direct Writing: A unique technique for grating component fabrication is to make use of EB-induced refractive index change. Amorphous chalcogenide thin films such as As–S and As–Se–S–Ge systems suitable for waveguides exhibit large index changes by an EB irradiation [23] as shown in Fig. 9. Therefore, optical components in the form of refractive-index modulation can be "written" directly in the film without any other process, i.e., without mask, resist, development, and etching [24]. Graded-index structures can also be written since the index increment can be continuously controlled by the EB dose. The resistless EB "direct" writing technique has been applied to fabricate grating components in waveguides [25]–[27]. Grating fabrication in a polymer (PMMA) waveguide by the same technique has also been reported [28].

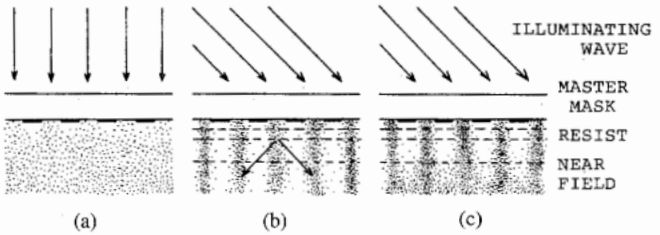

Fig. 10. Near fields of a grating under various illumination conditions. (a) Normal illumination, (b) oblique coherent illumination, (c) oblique incoherent illumination.

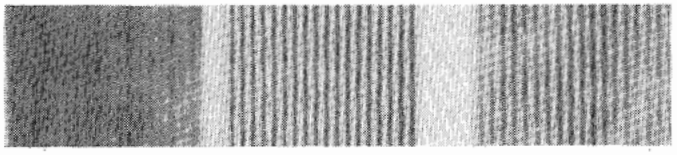

Fig. 11. Results of the preliminary experiment on holographic contact printing of a grating. (a) Near field pattern of master mask under the illumination Fig. 10(a), (b) near field pattern of master mask under the illumination Fig. 10(c), (c) grating copied and observed by illumination Fig. 10(c).

D. Optical Duplication

The major drawback of EB writing is the rather low throughput. It is therefore important to have an economical means for duplication from the production point of view. An optical means using photoresist would be preferable because of the IC process compatibility. The conventional photomask printing, however, cannot work effectively with the submicron patterns because of the resolution limited by diffraction. But as far as periodic patterns are concerned, positive use of the diffraction effect can be made; the technique developed for hologram copying can be applied effectively. Fig. 10 illustrates the holographic contact printing technique [29], [30] applied to the grating photomask duplication. The ordinary normal illumination of submicron grating photomask results in a blurred near field (a). The inclined coherent (laser) illumination yields the first-order diffracted light, and the transmitted and diffracted light interfere to form a high-visibility fringe (b). Even with incoherent illumination, the fringe is formed in the near field where the path difference is within the short coherence length (c). Therefore, the grating pattern can be copied in a photoresist in the near field. A master mask of the phase type can be used as well as the absorption type. The diffraction theory shows that the minimum grating period which can be copied with the illuminating wavelength λ_c is given by $\Lambda_{\min} = \lambda_c/2$; this implies that most of the grating patterns for integrated optics can possibly be duplicated by employing the conventional apparatus having a mercury lamp only with the modification in the light incident angle. It is also important to note that all the phase modulations of the EB-written master pattern are transferred, and therefore the advantages described in Section III-A are reserved in the copy. The possibility of this technique has been confirmed by a preliminary experiment using a 0.4 μm period EB-written Cr master grating and a mercury lamp. Results are shown in Fig. 11.

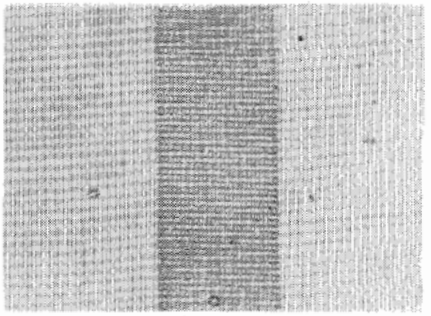

Fig. 12. Interference microphotograph of a transmission Bragg grating deflector [25].

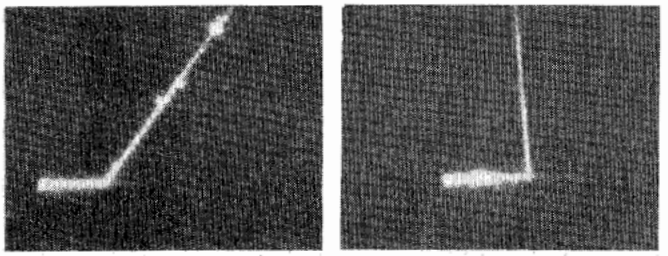

Fig. 13. Guided beam deflection by reflection Bragg gratings [26].

IV. Passive Components

A. Bragg Gratings for Deflection and Splitting

Coplanar Bragg gratings are simple and important components. Gratings of prescribed efficiency and selectivity can be designed by determining the coupling length L and coefficient κ (index-modulation) using (9)–(13). Various gratings were fabricated by the EB direct writing technique in $As_2S_3/SiO_2/Si$ waveguides.

1) Transmission Type: Fig. 12 shows an interference microphotograph of a transmission grating deflector [25]. The deflector function, and the power splitting function with about 50 percent efficiency, were experimentally confirmed. The transmission Bragg gratings are suitable for modulating the structure to add various wavefront conversion functions as will be seen in Section IV-B3) and Section VI-E, although it is not easy to obtain a very high efficiency.

2) Reflection Type: It is noted from (10) and (13) that the efficiency η aproaches asymptotically to 100 percent with increasing κL for reflection gratings, while η takes 100 percent only at discrete values of κL ($\nu = \pi/2, 3\pi/2, \cdots$) for transmission gratings. Thus, the realization of a high efficiency is easier with reflection gratings if the deviation of κL from the designed value is taken into account. Reflection-type grating deflectors of 0.5 and 0.34 μm periods were fabricated [26]. Wide angle deflections with almost 100 percent efficiencies were obtained as shown in Fig. 13. The typical angular bandwidth was 0.3°. The coupling coefficient of coplanar diffraction is approximately proportional to $\cos \theta_{di}$ for the TE mode and independent of θ_{di} for the TM mode, where $\theta_{di} = \theta_d - \theta_i$ is the deflection angle; this implies that a grating of near-right-angle deflection serves as a TE–TM mode splitter. The polarization splitter function was also experimentally confirmed [26].

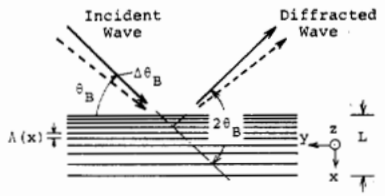

Fig. 14. Chirped Bragg grating for wide-band deflection [26].

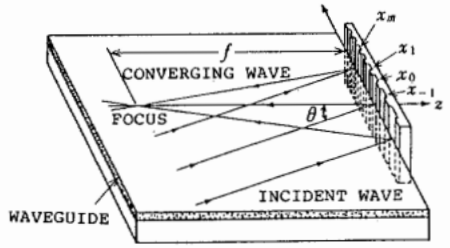

Fig. 15. Reflection-type chirped grating lens butt coupled to a waveguide.

3) Chirped Gratings: There are many applications where the angular and wavelength selectivities of Bragg gratings should be reduced to have a larger acceptance angle and/or a broad spectral bandwidth. Such wide-band characteristics can be realized in a chirped grating as shown in Fig. 14. An incident wave is diffracted within a portion of the grating where the beam angle and the wavelength satisfy the Bragg condition with the local grating constant. Linearly-chirped gratings of 0.5 μm center period, 0.05–0.2 chirp rate, and 500–1000 line number were fabricated [26]. Characteristics of angular acceptance of 3.5°, 2°, and a wavelength bandwidth of 1000 Å, which are in good agreement with the theoretical prediction, were obtained with efficiency of 50–95 percent.

B. Waveguide Lenses

1) Requirements and Problems of Waveguide Lenses: Waveguide lenses are an extremely important component for integrated optics since they perform various functions of imaging, collimating, focusing, and Fourier transforming on a guided wave. For many applications, the waveguide lenses must exhibit excellent performances such as diffraction-limited and aberration-free focusing characteristics, high efficiency, and large angle of view. The requirements are stringent, especially in constructing optical IC's for signal processing, such as RF spectrum analyzers. Because of the important functions and the difficulty in satisfying the requirements, waveguide lenses have been considered to be a key component for integrated optics [31], [32].

Mode-index lenses corresponding to singlets, fabricated in earlier work, exhibited large aberrations. Good performances have been achieved in Luneburg lenses and geodesic lenses. But these waveguide lenses involve difficulty of fabrication; Luneburg lenses require a high-precision gradient-thickness deposition process and geodesic lenses require an expensive and time-consuming precision mechanical grinding process. In addition, Luneburg lenses have limited focusing capabilities in high index waveguides where appropriate higher index cladding materials are difficult to find. Another problem of waveguide lenses arises from the necessary integration in a waveguide with other components. The possible deviation in focal length from the designed value, which is tolerated in conventional and microoptics, is fatal in integrated optics because the positions of all of the components are rigidly fixed.

There has been much interest in diffraction-type waveguide lenses, i.e., grating lenses and Fresnel lenses, since they eliminate many of the above-described problems. The major advantage of diffraction lenses is that they can be fabricated by the planar microfabrication technique. The designing is simple because of the inherent aberration-free characteristics. The focusing characteristics (focal length) are determined by the planar lens pattern (in particular, the periodicity) and are insensitive to fabrication process variations; the focal length control is easy and highly reproducible.

2) Reflection Chirped Grating Lenses Butt Coupled to Waveguides: The easiest introduction of diffraction grating to integrated optics is to use a conventional reflection-type grating and butt couple it to a polished waveguide edge. When the period of the grating is chirped, the input guided wave undergoes a wavefront conversion through the diffraction. Thus, it is possible to design and fabricate a grating which serves as a lens for guided waves [33]. Fig. 15 shows schematically a reflection chirped grating lens butt coupled to a waveguide, which is not exactly a waveguide lens but is equivalent in function. The lens, being of reflection type, should have an off-axis configuration for the spatial separation of the optical axes of the input and output waves. The periodic structure is designed by calculating the phase difference between the input and output wavefronts. For a lens which focuses a parallel wave of incident angle θ into a point on axis normal to the grating plane as shown in Fig. 15, for example, the phase difference can be written as

$$\Delta\Phi(x) = [kn_e(f - \sqrt{x^2 + f^2})] - [(kn_e \sin\theta)x] \quad (21)$$

where f is the focal length and n_e is the mode index, and therefore from (20), the mth grating line boundaries are specified by $\Delta\Phi(x_m) = 2m\pi$.

The efficiency of the lens can be calculated by the theory of thin gratings. For a (chirped) lamelar grating having rectangular cross section, the efficiency is given by

$$\eta = (4R/\pi^2) \sin^2 [(\pi/2)(4n_g d/\lambda)] \quad (22)$$

where d, R, n_g are the groove depth, surface reflectivity, and the refractive index of the medium filling the groove (optical bond), respectively, and η takes the maximum of 40.5 percent when $d = \lambda/4n_g$ and $R = 1$. The grating lens of this type has a very large acceptance angle and can easily be fabricated. Lenses of F/3-5, exhibiting performance comparable to the theoretical prediction, have been fabircated on Si substrates by EB writing, reactive ion etching of Si–N overlay, and depositing Al reflection coating. To have a higher efficiency, the grating must be blazed to be an echellette grating having triangular cross

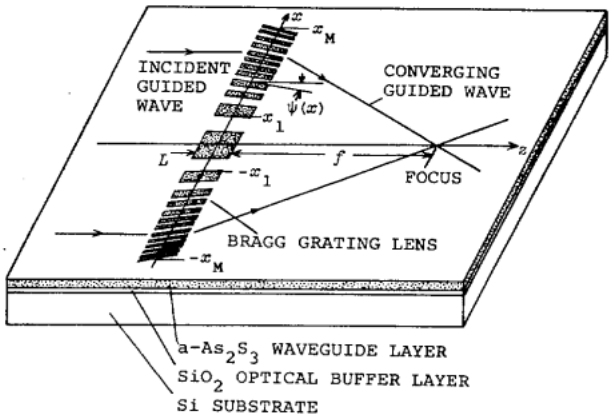

Fig. 16. Waveguide chirped Bragg grating lens.

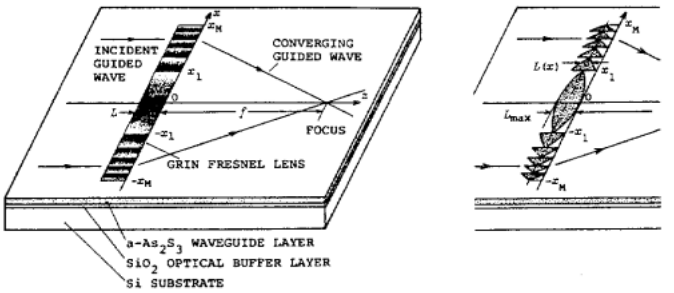

Fig. 17. Waveguide Fresnel lenses. (a) Gradient-index (GRIN) Fresnel lens, (b) gradient-thickness (GRTH) Fresnel lens [42].

section. To do this, the ion-beam etching technique or the gradient-dose technique (Section III-C) can be employed; using the latter, efficiencies up to 70 percent have been obtained for gratings of comparatively large ($\gtrsim 2$ μm) period [34].

3) Chirped Bragg Grating Lenses: Fig. 16 shows a chirped Bragg grating lens configuration. A lens having a focal length f should impose the phase modulation to convert a 2-D plane wave into a converging 2-D cylindrical wave:

$$\Delta\Phi(x) = kn_e(f - \sqrt{x^2 + f^2}) \simeq -(kn_e/2f)x^2. \quad (23)$$

Chirped grating lenses give the corresponding modulation

$$\begin{aligned}\Delta n(x) &= \Delta n \cos [\Delta\Phi(x)] \\ &= \Delta n \cos [kn_e(f - \sqrt{x^2 + f^2})]\end{aligned} \quad (24)$$

to the mode index on the lens aperture. To have a high efficiency, the grating must be of the "thick" Bragg type satisfying $Q \gtrsim 10$ with the Q parameter defined by (3), and the grating lines should be gradiently slanted as

$$\psi(x) = (\tfrac{1}{2}) \tan^{-1} (x/f) \simeq x/2f \quad (25)$$

so that the Bragg condition is satisfied over the whole aperture. The diffraction-limited 3 dB spot width of the main lobe on the focal line is given by

$$2\sigma = 2(f/n_e k x_M) \cdot 1.38 = 0.88F\lambda/n_e \quad (26)$$

where $2x_M$ is the aperture and $F = f/2x_M$ is the F number. The condition for maximizing the efficiency can be written from (10) as

$$\kappa L = \pi\Delta nL/\lambda = \pi/2. \quad (27)$$

The index modulation can be of the step type as shown in Fig. 16, instead of the sinusoidal type given by (24); then the amplitude of the fundamental Fourier component in (1) should be used for Δn in (27).

The in-line configuration shown in Fig. 16 has the drawback that $Q \gtrsim 10$ cannot be satisfied in the central portion, although it is advantageous to have a small F number. The lens portion satisfying $Q \gtrsim 10$ only can be fabricated to have an off-axis lens. There have been many experimental works on chirped Bragg grating lenses of in-line and off-axis types. Lenses of 1–3 mm aperture and F/3-10 have been fabricated in glass waveguides by etching and cladding [35], [36] in $As_2S_3/SiO_2/Si$ waveguides by the EB direct writing technique (see Fig. 18, the **Tilt* function used) [37] and in $LiNbO_3$ waveguides by etching, cladding, and proton-exchange techniques [38]–[40]. Nearly diffraction-limited focusing and efficiencies of 50–90 percent have been obtained.

4) Fresnel Waveguide Lenses: Fig. 17 shows the waveguide Fresnel lens configurations. Fresnel lenses give a phase modulation equivalent to (23):

$$\begin{aligned}&\Phi_F(x) = \Delta\Phi(x) + 2m\pi, \\ &\qquad \text{for } x_m < |x| < x_{m+1},\ \Delta\Phi(x_m) = -2m\pi,\end{aligned} \quad (28)$$

which is obtained by segmenting the modulation $\Delta\Phi(x)$ into zones so that Φ_F may have amplitude of 2π. In (28), x_m denotes the zone edge. Under the assumption of "thin" lens, the phase shift is given by $k\,\Delta n\,L$. Therefore, Fresnel lenses can be constructed by modulating Δn or L; the gradient-index (GRIN) Fresnel lens [Fig. 17 (a)] is described by

$$\Delta n(x) = \Delta n_{\max}[\Phi_F(x)/2\pi + 1], \qquad L = \text{const.} \quad (29)$$

and the gradient-thickness (GRTH) Fresnel lens [Fig. 17 (b)] is described by

$$L(x) = L_{\max}[\Phi_F(x)/2\pi + 1], \qquad \Delta n = \text{const.} \quad (30)$$

To have the modulo 2π phase modulation, in either case, the modulation amplitude must be optimized so that $k\Delta n_{\max}L = 2\pi$ or $k\Delta nL_{\max} = 2\pi$ is satisfied. The binary approximation of the phase modulation results in the step-index (SI) Fresnel zone lens.

Theoretical analysis of a "thin" SI Fresnel zone lens [41] and GRIN and GRTH Fresnel waveguide lenses [42] have been made based upon the scaler diffraction theory. The diffraction-limited focus spot width is given by (26). Fig. 18 shows the calculated intensity profile on the focal line. The parameter l denotes the ratio of the modulation amplitude to the above-given optimum value. The spot width is approximately independent of l, i.e., the diffraction-limited width is obtainable even in lenses of $l \neq 1$ and the SI lens. Fig. 19 shows the calculated dependence of the lens efficiency, defined as the ratio of the power in

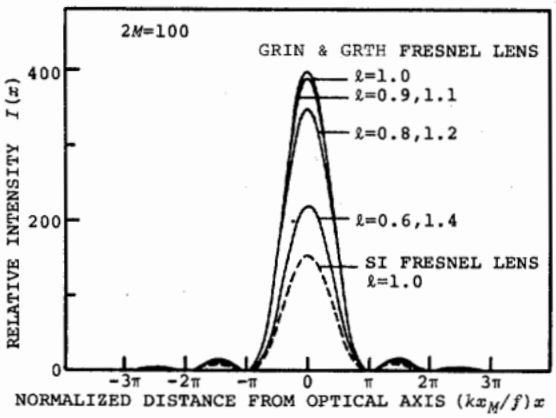

Fig. 18. Light intensity profiles on the focal line of Fresnel lenses [42].

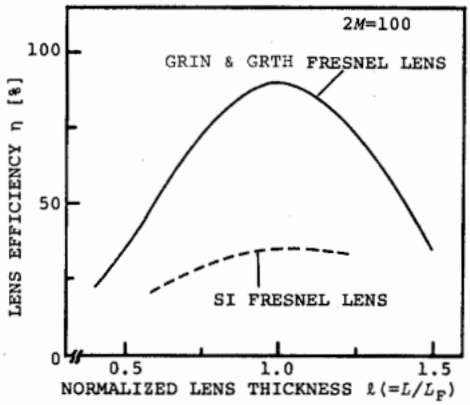

Fig. 19. Dependence of efficiency of Fresnel lenses upon the phase modulation amplitude [42].

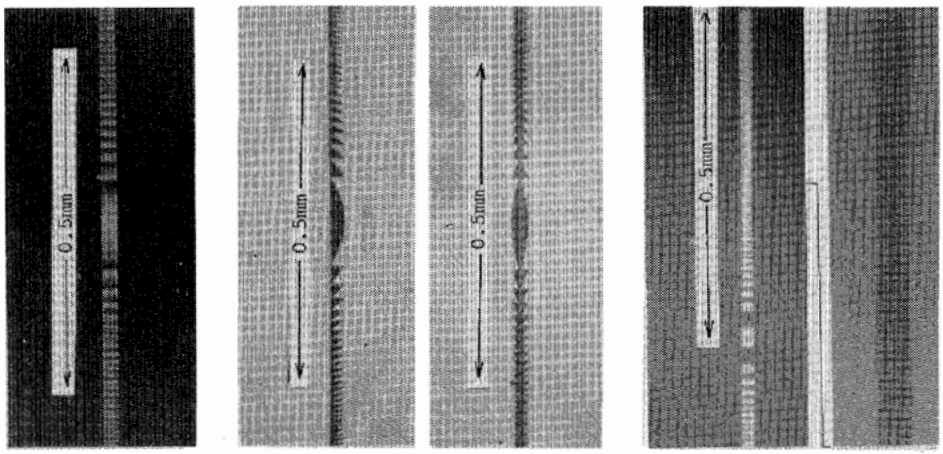

Fig. 20. Interference microphotographs of diffraction waveguide lenses. (a) GRIN Fresnel lens, (b) GRTH Fresnel lenses, (c) chirped Bragg grating lens.

the focus main lobe to the total input power, on the parameter l. The maximum efficiency of 90.2 percent, limited only by diffraction, can be obtained in GRIN and GRTH lenses, while the maximum efficiency for an SI Fresnel zone lens is 35 percent.

By using (3) and (28)–(30), the maximum of the Q parameter for the optimum modulation amplitude can be written as

$$Q_{\max} = (\pi/2)(\Delta n/n_e)^{-1}F^{-2} \tag{31}$$

and the condition for the ''thin'' lens $Q_{\max} < 1$ is given by

$$\Delta n/n_e > (\pi/2)F^{-2}. \tag{32}$$

This shows that, e.g., at least 6.3 percent mode index change is required for a lens of $F/5$. It is important to note that a lens which does not satisfy (32) is not ''thin'' and suffers from a reduction of efficiency.

The feasibility of diffraction-type waveguide lenses by lithography was first proposed and demonstrated with SI Fresnel zone lenses ($F/2.5$, 5, efficiency of 23 percent) in a BaO waveguide on glass substrate with CeO overlay cladding which was patterned by photolithography using an EB written photomask [41]. The same kind of lens (f = 10.2 mm, $F/8.5$, efficiency 19 percent) has been fabricated by patterned cladding of SiO_2 in an $Si_3N_4/SiO_2/Si$ waveguide, which is more suitable for integration [43].

High-efficiency GRIN and GRTH Fresnel lenses have been demonstrated using $As_2S_3/SiO_2/Si$ waveguides [37], [42]. By the EB direct writing technique, GRIN and GRTH lenses of 1 mm aperture, $F/3$, and $F/5$ were fabricated. The electron beam was scanned along the optical-axis direction with small scanning line displacements (0.1 μm) so that the beam traces may overlap. For a GRIN lens, the scanning speed or the number of scanning repetitions on a line was varied to give the gradient dose distribution, and for GRTH lens, the scanning width was varied using the *X-$Scan$ B function to write the GRTH pattern. Fig. 20 shows the interference microphotographs of the fabricated lenses. The nearly diffraction-limited focusing characteristics (3 dB width of 3.5 μm for $F/5$, λ = 1.06 μm, and 3.7 μm for $F/5$, λ = 0.83 μm) and the efficiency up to 61 percent have been obtained.

The GRTH Fresnel lenses were fabricated also in an $Si_3N_4/SiO_2/Si$ waveguide with SiO_2 overlay cladding patterned by standard photolithography [44]. In the struc-

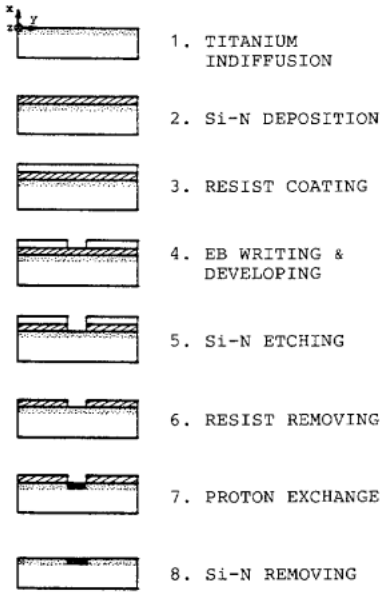

Fig. 21. Fabrication process of proton-exchanged Fresnel lenses in Ti : $LiNbO_3$ waveguides.

ture, the mode index change up to approximately 0.032 was available, and nearly diffraction-limited focusing characteristics and efficiencies of 60–70 percent were reported with lenses of F numbers around 6.

Realization of high-performance waveguide lenses in $LiNbO_3$ has been strongly desired since the $LiNbO_3$ is considered to be one of the most suitable waveguide material for optical IC's. Fabrication of Fresnel lenses, however, has not been reported until recently because of the difficulty in obtaining the required large index change. Most recently, the proton-exchange technique [45], which gives an index change as large as 0.11, was applied to fabricate a GRTH Fresnel lens in a Ti-indiffused $LiNbO_3$ waveguide [46]. The fabrication process is shown in Fig. 21. The waveguide was coated with a thin Si–N mask layer and the lens pattern written by EB was transferred to the mask layer by reactive ion etching. The waveguide was then immersed in moleten benzoic acid for the patterned proton exchanging. The nearly diffraction-limited focusing properties and efficiencies as high as 70 percent have been obtained in the lenses of $F/5$.

C. Grating Couplers

1) Input/Output Couplers: Grating couplers have been widely used to excite and take out a guided wave [1]–[5]. The earlier works on EB written gratings aimed at fabrication of grating couplers [47], [48]. To have a high efficiency, the fractional power P_q^i in (16) should be maximized for a required q-i radiation. In the two-beam coupler with a transparent substrate [Fig. 4 (b)], however, the output is divided into approximately halves for air and substrate. Methods to eliminate unnecessary radiation and maximize P_q^i for the necessary output beam include the use of the backward substrate radiation [49] and the use of blazed gratings [50]. The use of a reflective substrate can be another method to improve the situation. Fig. 22 shows the dependences of the fractional air power and the radiation decay factor on the device parameters, calculated for a grating coupler on a glass/SiO_2/Si waveguide. The fractional power is a periodical function of the buffer layer thickness t_b; the air power can be enhanced by choosing t_b to add constructively the reflected substrate radiation to the air radiation. It is seen from (16) and Fig. 22 that approximately 60 percent efficiency can be obtained for $\alpha_r L = 1$. Based upon this design, grating couplers have been fabricated by EB writing [51], [52]. The pattern was transferred to a thin Si–N cladding layer on the waveguide to form the grating. Output efficiencies around 50 percent were obtained with 1×1 mm^2 area gratings.

2) Focusing Grating Couplers: The possibility of adding a complex wavefront conversion to a grating coupler was first demonstrated in waveguide holograms [53], which aimed at an approach to hologram integration. A pictorial image was recorded by interference and reconstructed by a guided wave. A special example of waveguide holograms is a focusing grating coupler (FGC) shown in Fig. 23, where the object is a point image. The FGC incorporates the coupling and the focusing, and therefore has many applications, e.g., guide to LD or fiber couplers and ones presented in the following sections.

Focusing grating couplers were fabricated by the holographic technique [54]. But they exhibited large aberrations, except for ones with a small aperture, due to the difference in wavelength between the fabrication and coupling lights. The EB writing is required to fabricate aberration-free FGC's. A low-periodicity FGC with the focusing beam in the substrate was fabricated by EB writing in a polymer waveguide [55].

High-periodicity FGC's with the focusing beam in air as shown in Fig. 23 were fabricated by EB writing in glass/SiO_2/Si waveguide [51], [52]. The pattern is specified from (20) by

$$\Delta\Phi(x, y) = kn_e y + k\sqrt{x^2 + (y - f\sin\theta)^2 + (f\cos\theta)^2} = 2m\pi + \text{const.} \quad (33)$$

where θ is the output beam angle. An important requirement of FGC's is that the radiation decay factor should satisfy the condition $\alpha_r L = 1$ to realize a high efficiency and the minimum focus spot width simultaneously; too large a decay factor results in the reduction of the effective aperture and therefore in the broadening of the spot size. The FGC's were designed by using Fig. 22 and (16) and fabricated by the curved-line scanning of EB using the *X-$Scan$ B function. Fig. 24 shows the focus spot and the intensity distribution. Efficiency of approximately 40 percent and a focus spot width of 1.4 μm (diffraction-limited value 1.1 μm) have been obtained with FGC's of $f =$ 2 mm and 1×1 mm^2 area.

D. Channel Waveguide Array

Coplanar periodic arrays of channel waveguides are an important component for integrated optics. An array with

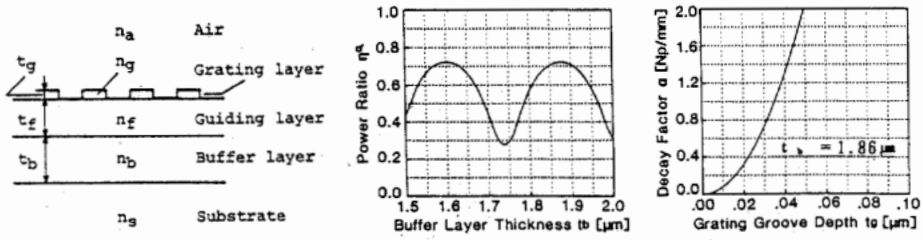

(a) (b) (c)

Fig. 22. Grating coupler on reflective substrate. (a) Cross section, (b) dependence of the fractional air power on the buffer layer thickness, (c) dependence of the radiation de... ...ie grating groove depth.

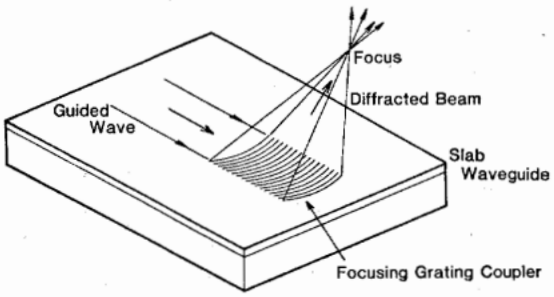

Fig. 23. A focusing grating coupler configuration.

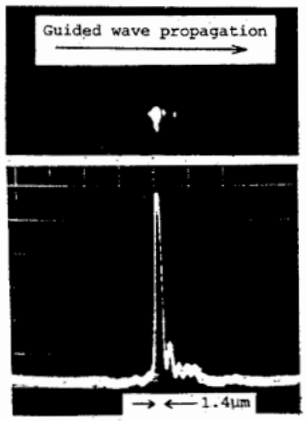

Fig. 24. Focus spot and the intensity profile of a focusing grating coupler.

interchannel distributed coupling which takes place between adjacent channels with modal field ovelap, i.e., a multichannel directional coupler, has been reported with the power branching/distributing function [56]. Arrays without interchannel coupling also have many applications, e.g., spatial sampling, transmission, imaging of one-dimensional spatial light signals, and as an interface element in multichannel parallel signal processing devices. The spatial magnifier (expander) function can also be incorporated when the channels are gradiently tilted towards each other to be a fan-out configuration. Ridge channel guides are advantageous for obtaining small crosstalk between channels with small spacing. A polymer fan-out array on Si substrate with an integrated photodetector array has been fabricated [57]. Fig. 25 shows a fan-out channel guide array [58], where a high-index Si–N ridge guide on an SiO_2/Si substrate is adopted to have a large numerical aperture needed for efficient butt coupling. The pattern was written by an electron beam with the **Tilt* function, and then transferred to the guide layer by reactive ion etching to form the ridge channels. In the fabricated 200-channel array with 3× magnification, a crosstalk level for two adjacent guides of less than −20 dB has been obtained.

V. Elements for Guided-Wave Modulations and Detection

Many integrated optics devices require elements for guided-wave modulation and detection. Periodic structures also play an important role in such elements. Spatially periodic modulations in the refractive index induced in a waveguide through acoustooptic or electrooptic effects are electrically controllable and enable the temporal and spatial modulation of guided waves. Such waveguide modulator elements of the coplanar configuration will be discussed here, although the collinear and radiation configurations also have many applications.

A. Acoustooptic Bragg Cells

An acoustooptic (AO) Bragg cell [59], [60] is constructed with a surface acoustic wave (SAW) transducer and an AO interaction region on a planar waveguide as shown in Fig. 26. The unique and important features of the AO gratings induced by SAW are that 1) the grating period can be continuously changed by the frequency of the input RF signal, and 2) the serial input signal is converted into a spatial parallel signal through the SAW propagation effect. This assures a variety of applications in waveguide optical signal processing, e.g., modulators/switches, variable angle deflectors (guided beam steering), tunable optical filters, and spatial light modulators [60]. It is also important to note that an AO grating, not being fixed but traveling, causes a Doppler shift on the diffracted wave, and therefore a Bragg cell serves as an optical frequency shifter.

Recent research activities on waveguide AO Bragg cells are directed towards achieving wide-band operation together with high efficiency and low drive power [60]. The piezoelectric $LiNbO_3$ crystal is considered to be the best waveguide material for this purpose because of the excellent SAW propagation and AO characteristics in the high-frequency range, whereas other thin-film waveguides can

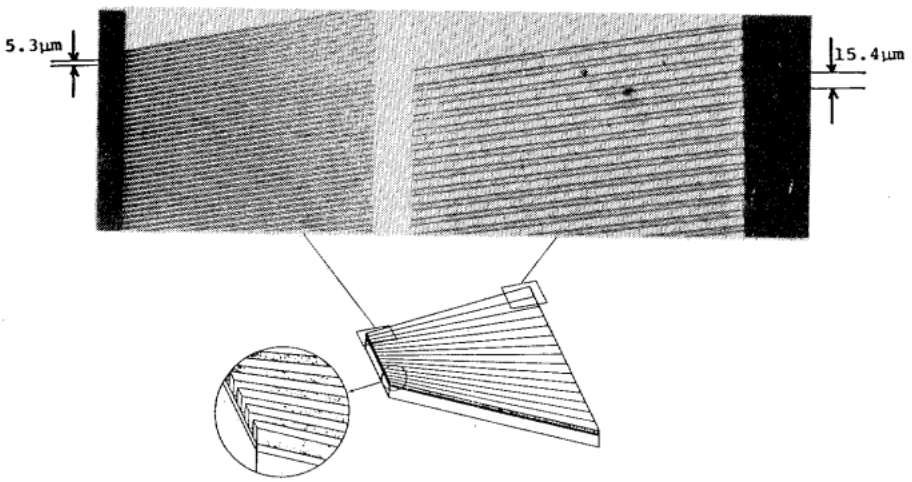

Fig. 25. A fan-out channel waveguide array.

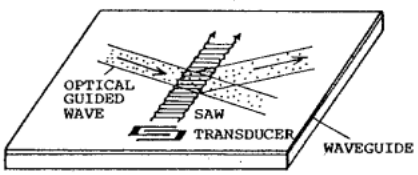

Fig. 26. Fundamental configuration of a waveguide acoustooptic Bragg cell.

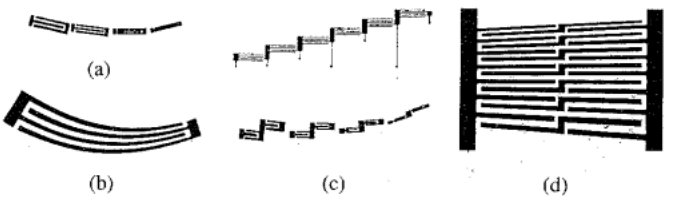

Fig. 27. Interdigital SAW transducers for wide-band waveguide Bragg cells. (a) Multiple tilted array transducers, (b) curved finger transducer, (c) phased array transducers, (d) tilted-finger chirped transducer.

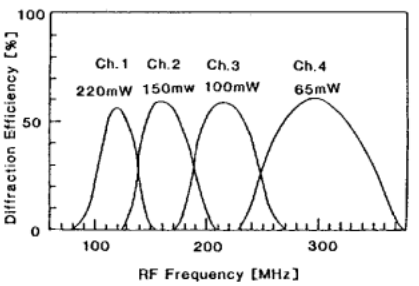

Fig. 28. Frequency response of a waveguide Bragg cell using multiple tilted array transducers.

preferably be used with thin-film SAW transducers for monolithic integration on an Si substrate [61], [62].

Since the Bragg condition (4) can be rewritten as

$$2kn_e \sin \theta_B = K, \qquad k = 2\pi/\lambda,\ K = 2\pi/\Lambda, \tag{34}$$

for the first-order diffraction without mode conversion, the deflection angle $2\theta_B$ is given by

$$2\theta_B = 2 \sin^{-1} (\lambda/2n_e\Lambda) \simeq \lambda\nu/n_e v \tag{35}$$

with the frequency ν, the period Λ, and the phase velocity v of the SAW, and is approximately proportional to the SAW frequency.

The diffraction efficiency ζ of a Bragg cell can be written, by using (5), (6), (8), and (9) for $\phi = \pi/2$, $q = 1$, $\beta_i = \beta_d = 2\pi n_e/\lambda$, $\theta_{iB} = -\theta_{dB} = \theta_B$, and making a calculation of the coupling coefficient κ [60], as

$$\zeta = [\sin^2 (g^2 + \xi^2)^{1/2}]/[1 + \xi^2/g^2] \tag{36}$$

$$g^2 = (\pi^2/4\lambda^2)(n_e^6\Gamma^2L^2/\cos^2 \theta_B) \tag{37}$$

$$\xi = K\Delta\theta L/2, \qquad \Delta\theta = \theta - \theta_B \tag{38}$$

where L denotes the width of the acoustic wave, θ is the incident angle of the guided wave, and $\Delta\theta$ is the deviation of θ from the Bragg angle. The parameter Γ^2, being the overlap integral of the guided wave and SAW field profiles, is proportional to the SAW power and therefore to the input driving RF power [60].

The frequency bandwidth, i.e., the angular range of the beam steering, of Bragg cell is determined by the bandwidths of the SAW excitation and the AO interaction. Consider first a Bragg cell having a standard uniform-period interdigital SAW transducer (IDT), as shown in Fig. 26. To maximize the excitation bandwidth of such an IDT under the electric impedance matching condition, the IDT finger pair number N should be chosen to equalize the SAW synchronization bandwidth (proportional to N^{-1}) and the electrical bandwidth (proportional to N) [63]. When N is optimized by this method ($N = N_{opt}$), the SAW excitation bandwidth is given by

$$2\Delta\nu_1/\nu \simeq 1/N_{opt}. \tag{39}$$

The AO interaction bandwidth, on the other hand, is derived from (34)–(38) to be

$$2\Delta\nu_2/\nu \simeq (10n_e\Lambda/2\pi\lambda)(\Lambda/L). \tag{40}$$

The IDT aperture ratio L/Λ should be a constant value optimized for the electric impedance matching, and then $2\Delta\nu_2/\nu$ is inversely proportional to $\nu(=v/\Lambda)$. Therefore, the relative bandwidth of a Bragg cell is limited by the excitation bandwidth ($2\Delta\nu_1/\nu$) in the low-frequency range and by the interaction bandwidth ($2\Delta\nu_2/\nu$) in the high-frequency range.

To realize a wider bandwidth beyond the above limi-

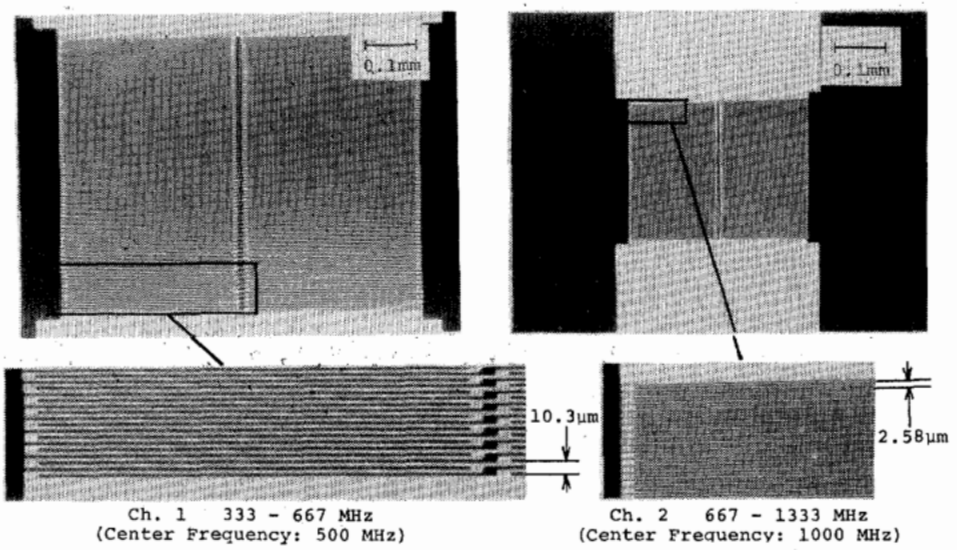

Fig. 29. Microphotograph of tilted-finger chirped transducers fabricated by electron-beam writing.

tations, modified IDT's for Bragg cells as shown in Fig. 27 have been proposed and demonstrated [60]. The multiple tilted array IDT shown in Fig. 27 (a) is an array of standard IDT's, having staggered center frequencies, and tilted towards each other for satisfying the Bragg conditions at each center frequency. Parallel driving using an RF power divider enables wide-band operation, depending on the number of array stages. Fig. 28 shows typical characteristics of a Bragg cell using this type of IDT fabricated by standard photolithography on a Ti : $LiNbO_3$ waveguide. The IDT has advantages of easy design and high diffraction efficiency, although the number of stages required for the wide-band operation increases rapidly in the high-frequency range where the relative interaction bandwidth becomes narrower.

The tilted-finger chirped IDT shown in Fig. 27 (d) broadens the excitation bandwidth by the chirp in electrode period and realizes the interaction bandwidth equal to the excitation bandwidth by the frequency-controlled SAW beam steering to maintain the Bragg condition over the bandwidth. The electrode fingers should be gradiently tilted for the SAW beam steering and have the dog-leg structure for the impedance optimization. This IDT has an advantage that a bandwidth as wide as one octave per one stage can be obtained, even in the high-frequency range. The fabrication of IDT's for the gigahertz frequency range where the finger width falls in the submicron region requires EB direct writing. Fig. 29 shows a microphotograph of a tilted-finger chirped IDT fabricated by EB writing and liftoff techniques. The pattern was written by tilted line scanning of the electron beam by the **X-Scan B* and **Tilt* functions of the system shown in Fig. 6. Fig. 30 shows the characteristics of a Bragg cell in a Ti : $LiNbO_3$ waveguide used in an RF spectrum analyzer described in Section VI-C; 1 GHz bandwidth has been achieved with a two-channel array of this type of IDT [64].

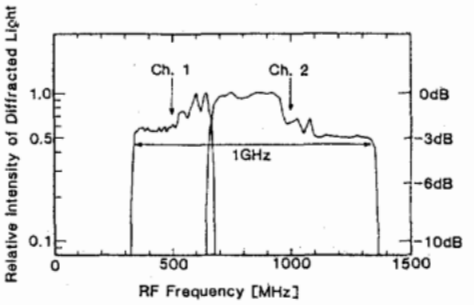

Fig. 30. Frequency response of a waveguide Bragg cell using the transducers shown in Fig. 29.

B. Electrooptic Grating Modulators

Periodic modulation in refractive index for coplanar Bragg diffraction also can be induced through the electrooptic (EO) effect by electric voltage applied to interdigital electrodes covering the interaction region. Waveguide modulators/switches based on such an EO grating were fabricated [65]. The EO grating elements are not capable of beam steering, i.e., the deflection angle is fixed, but they have the potential advantages of easy fabrication, high efficiency, and high-speed operation. The interdigital electrodes can be divided into segments having a small number of finger pairs to spatially modulate a guided wavefront. The resultant integrated optic spatial light modulators (IOSLM) have been fabricated and the many appications in signal processing have been demonstrated [66]. An EO controllable chirped grating lens has also been proposed and fabricated [67].

C. Integrated Photodetectors

In many integrated optics devices for optical communications and signal processing, the final output is required in the form of electric signals. Thus, photodetectors or photodetector arrays are essential components for such devices. The conventional detector devices can be

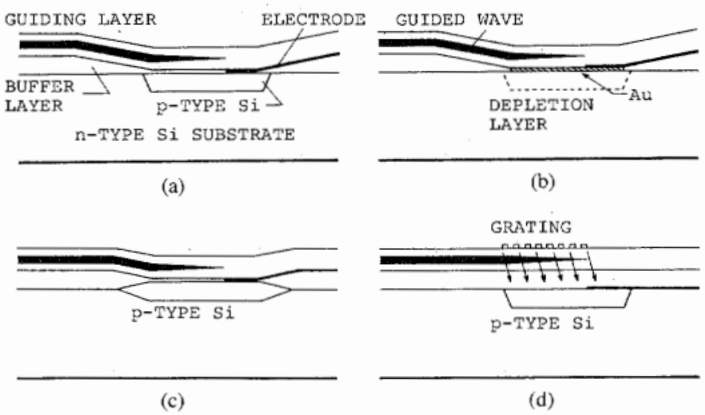

Fig. 31. Cross sections of integrated photodetectors. (a) Taper-coupled p-n photodiode, (b) taper-coupled Schottky barrier photodiode, (c) LOCOS-taper structure, (d) grating coupling structure.

used by hybrid coupling, but monolithic integration including detectors is desired to derive the advantages of integrated optics. Such integration is possible if SiO_2/Si is used as a substrate. The SiO_2 layer is thermally grown on Si for the optical buffer layer. The necessary monolithic waveguide to detector coupling has been of research interest [68], [69], whereas the fabrication of the detector element is an established semiconductor technology. Fig. 31 shows various cross-sectional configurations of integrated photodiodes. In the diode region, the light radiates by optical tunneling through the very thin SiO_2 layer into Si. The radiation decay length can be estimated by the theory of prism coupler [70]; the decay length can be designed to be roughly 0.1 mm for glass guides on SiO_2/Si. To lift the modal field adiabatically down to near the SiO_2/Si interface, the thickness of the buffer layer is tapered with a slope of around $\frac{1}{5}$. Such a taper in SiO_2 can be fabricated by chemical etching, associated with doping, ion implantation, or Si–N overlay deposition. These processes insert a very thin high-etch-rate layer between the SiO_2 and the resist mask, enhance the undercut, and result in taper etching. The local oxidization (LOCOS) technique with a patterned Si_3N_4 mask was used to fabricate the structure shown in Fig. 31 (c), and guide-to-diode coupling efficiencies higher than 90 percent were obtained with a 0.15 mm diode length. Fig. 31 (d) illustrates another possible coupling configuration using a grating. The guided wave is diffracted into SiO_2 as the first-order substrate radiation and then absorbed in Si. This configuration eliminates the need for the tapered transition region, and therefore can possibly be fabricated simultaneously with other grating components.

VI. Integrated Optic Devices

A. Guided-Beam Multidividers

The simplest integration of grating components is to combine several micrograting of the same type but with different specifications. Then the EB writing technique is advantageous because of the flexibility in the changing parameters, the easy framing of each element, and the possible precise registration of them. Fig. 32 shows an

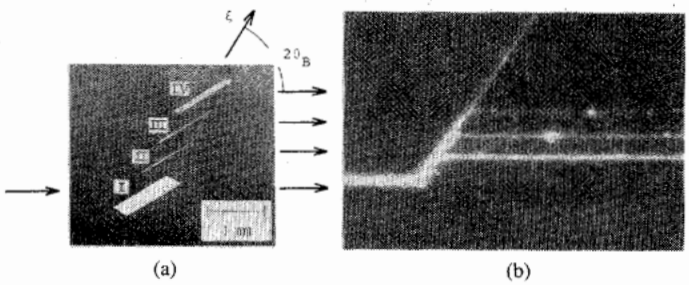

Fig. 32. An integrated grating circuit for guided-beam multiple division [71].

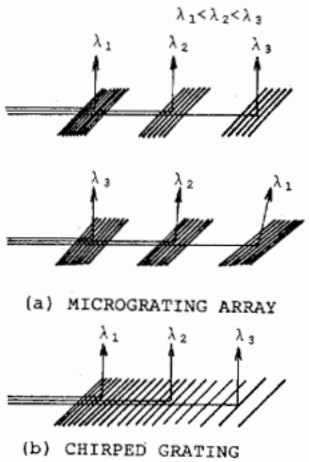

Fig. 33. Wavelength demultiplexer constructions using Bragg gratings.

integrated grating circuit (IGC) for guided-beam multiple division fabricated by EB direct writing in an As_2S_3 waveguide [71]. The IGC is composed of four coplanar Bragg gratings of reflection type; a chirped grating (**I**) having a wide acceptance angle is used at the first stage, and three uniform-period gratings (II-IV) divide the incident beam into three beams with prescribed ratios. The incident beam was deflected efficiently by the first chirped gratings and then divided into four output beams by the cascaded gratings.

B. Wavelength Multi- and Demultiplexers

The wavelength division multiplexing (WDM) is considered to be a promising technique to enhance the transmission capacity of an optical fiber communication system. In a WDM transmission system, wavelength multiplexers and demultiplexers are required to combine and separate wavelengths carrying different information. Integrated optic approaches have been made to construct compact multi/demultiplexers in a stable rugged structure with simplified assembling [72].

1) Single-Mode Waveguide Type: Wavelength multi/demultiplexing in a single-mode waveguide can be realized through the coplanar diffraction of guided waves by Bragg gratings fabricated in the waveguide. This type of grating diffracts the guided wave which satisfies the Bragg condition among the grating period, wavelength, and the incident angle of the guided wave. The separation of the optical axis is thus realized by the wavelength selectivity of the deflection. The demultiplexing of many wavelengths is realized by (a) a cascade array of micrograting

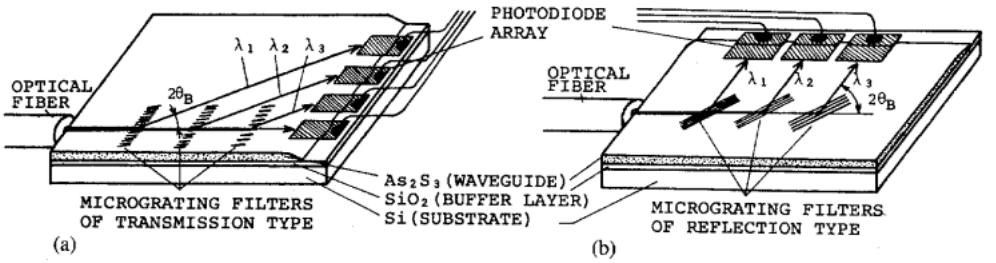

Fig. 34. Monolithic integrated WDM receiver terminals. (a) Transmission-grating type, (b) reflection-grating type [75].

with different periods or orientations or (b) a single chirped grating, as shown in Fig. 33. Experimental works have been made with a deflection-type grating filter for use in device (a); filtering characteristics of 0.6 Å bandwidth have been obtained with a grating fabricated by holographic lithography in a resist layer on a glass waveguide [73]. An experiment of demultiplexing five wavelengths with 50 Å separation has been reported with a chirped grating fabricated by etching in a glass waveguide [74].

In many applications of the demultiplexer, the demultiplexed components should be converted into electrical signals; the integration of the demultiplexer with photodetectors in one chip is desired. Such a monolithic integrated WDM receiver terminal is an example of an optical IC because it includes different kinds of components. Devices using a Si substrate have been proposed and fabricated. Fig. 34 shows devices constructed by the integration of a micrograting array demultiplexer fabricated by the EB direct writing in an $As_2S_3/SiO_2/Si$ waveguide and a Schottky barrier photodiode array fabricated on the Si substrate [75]. For efficient coupling between waveguide and photodiode, the SiO_2 buffer layer was etched to form the tapered coupling region as shown in Fig. 31 (b). In the fabricated prototype device for two wavelengths, the demultiplexing operation has been confirmed with a crosstalk less than -15 dB. The diffraction efficiencies of 45–75 percent and 90 percent have been obtained with the transmission-type gratings and reflection-type gratings, respectively.

A full-integrated WDM receiver terminal, wherein a chirped grating for demultiplexing, waveguide lenses for guided wave collimating and focusing, and a detecter array with processing electronics are included, has also been proposed [69]. The prototype device with a chirped grating has been fabricated by holographic lithography.

The design theory and the fabrication techniques of each component for the above-described single-mode monolithic WDM receiver have been almost established. However, further works, including the solution of the efficient fiber to waveguide coupling, are required before accomplishing the full-integrated devices and evaluating the ultimate overall performances.

2) Multimode Waveguide Type: Multi/demultiplexers for multimode fiber transmission systems should be constructed with a multimode waveguide to obtain efficient coupling to the fiber. The use of Bragg gratings in such a multimode waveguide is not effective since the Bragg condition cannot be satisfied simultaneously with all the modes due to the mode dispersion. The effective device construction for the grating demultiplexer is to make a two-dimensional version of an ordinary grating monochrometer by using a planar waveguide. Various configurations to realize the necessary lens function have been proposed and demonstrated.

The first device of a Roland configuration was fabricated by bonding a flexible grating sheet on a curve-polished edge of an ion-exchanged planar waveguide [76]. A blazed (echelette) grating is required to improve the diffraction efficiency. Such a device was fabricated by combining a sandwich-bonded glass waveguide and an aberration-corrected concave grating prepared by using a ruling engine. Demultiplexing of ten channels with 300 A separation and insertion loss less than 2.8 dB has been obtained [77]. A similar device of five channels with 1.8 dB insertion loss has also been fabricated by using an echelette grating produced by the anisotropic etching of Si [78]. The wavelength resolution can be improved by using the exact Roland circle configuration; a device of 100 Å channel separation has been realized [79]. These devices, however, have the drawback that they require time-consuming curved edge polishing.

The need for the focusing element (curved edge or lens) can be eliminated by using a chirped grating. Fig. 35 shows a demultiplexer constructed with an ion-exchanged waveguide and a reflection-type chirped grating [80]. The input light diverging into the slab guide after transmission through the input channel is diffracted by the chirped grating and focused at the slab/output-channel interfaces. The diffraction angle and the focal length depend upon the wavelength; the demultiplexing function is realized by patterning the waveguide so that the slab/channel interfaces of each output channel may coincide with the focal points for the corresponding channel wavelength. A demultiplexer having five output channels with a wavelength separation of 300 Å in the 1 μm band was fabricated. The measured demultiplexing characteristics are shown in Fig. 35 (b). The crosstalk between adjacent channels was less than -21.5 dB and the total insertion loss was measured as 9.5 dB. The rather large insertion loss is due to the low efficiency of the lamelar grating; an improvement should be made by blazing.

A demultiplexer of the Litrrow configuration can be constructed using a waveguide lens [81]. Among various

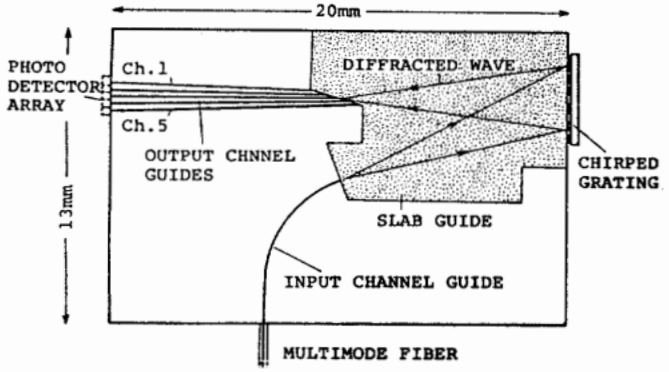

(a)

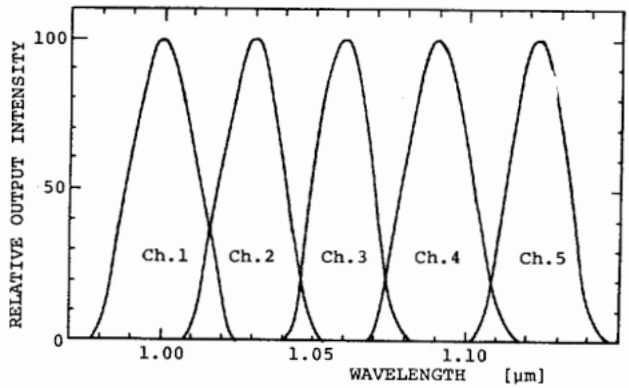

(b)

Fig. 35. An integrated optic wavelength demultiplexer using a chirped grating and an ion-exchanged waveguide. (a) Device configuration, (b) demultiplexing characteristic [80].

waveguide lenses, only a geodesic lens can perform well in a multimode waveguide since it exhibits no chromatic and mode aberrations. Such a multimode geodesic lens can be fabricated in glass (ion-exchanged) waveguides by thermal pressing techniques [82], [83], and ordinary echelette grating can be butt coupled to construct a demultiplexer. A six-channel (350 Å separation) demultiplexer with approximately 4 dB insertion loss has been reported [81].

The last two devices require no curved edge polishing, and therefore they are suitable for economical mass production.

In contrast to the single-mode type, the techniques of the multimode-type devices almost have been established, although some improvements are still required in the insertion losses and the fabrication processes. They possibly will be brought to practical applications in the near future.

C. Integrated Optic RF Spectrum Analyzers

A real-time spectrum analysis of wide-band RF signals is required in radar signal processing, signal processing for radio astronomy, and future laser optical measurement systems, etc. An integrated optic RF spectrum analyzer (IOSA) is constructed by integrating an acoustooptic Bragg cell and a pair of waveguide lenses for guided-beam collimating and Fourier transforming [60]. A LD light source and a photodetector array should be coupled to the waveguide input and output ends, respectively. In the

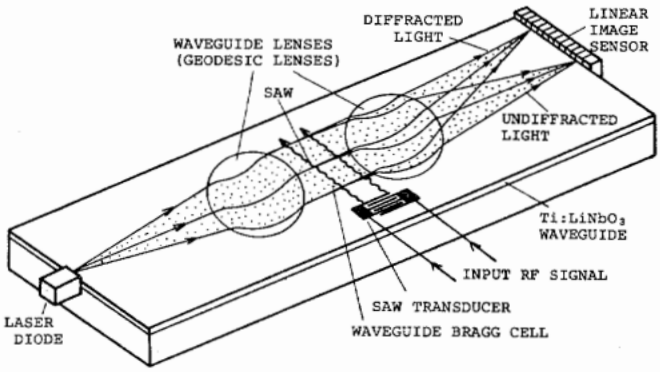

Fig. 36. An integrated optic RF spectrum analyzer using geodesic lenses.

Bragg cell, the guided wave is deflected at an angle proportional to the frequency of the RF signal fed into the SAW transducer, and the diffraction efficiency is approximately proportional to the input RF power. Therefore, after the Fourier transformation of the guided wave by the waveguide lens, the power frequency spectrum of the input RF signal is obtained on the photodetector array in the form of the light intensity distribution.

1) Wide-band IOSA's Using a $LiNbO_3$ Waveguide: A $LiNbO_3$ crystal is considered to be the most promising waveguide material for a wide-band IOSA since it exhibits excellent SAW propagation and acoustooptic characteristics at high frequency. The theoretical considerations show that an IOSA of 1 GHz bandwidth, 1 MHz resolution, and 1 μs response time is feasible [60], [84]. The key component for constructing the IOSA is the waveguide lens. Various types of IOSA using geodesic lenses, Luneburg lenses, and diffraction lenses have been proposed, fabricated, and tested.

Fig. 36 shows an IOSA using geodesic lenses. Many research groups have been involved in the fabrication of this type of ISOA, and the fully integrated devices (with the LD and the photodetectors) have been demonstrated [84], [85]. The geodesic lenses are fabricated by the computer numerical control diamond turning method. The typical performances reported so far are 200–500 MHz bandwidth, 4–8 MHz resolution, 2 μs response time, and dynamic ranges in excess of 20 dB. A resolution of 2.7 MHz has been obtained by using a Fourier transform lens of long (53 mm) focal length [86]. For practical application, the achievement of a large dynamic range is of great importance. So far, a dynamic range in excess of 40 dB has been reported [87]. As seen from these examples, the design theory and the fabrication techniques of the IOSA with geodesic lenses have been almost established. An IOSA using Luneburg lenses has also been fabricated [88]. However, these lenses involve the problems as pointed out in Section IV-B.

The alternative waveguide lenses for IOSA's are diffraction lenses. An IOSA construction using grating components has been considered [89]. Fig. 37 shows a folded-type IOSA using reflection-type chirped grating lenses (CGL's) butt coupled to the waveguide [64], [90]. The grating lenses can easily be fabricated by the EB writing

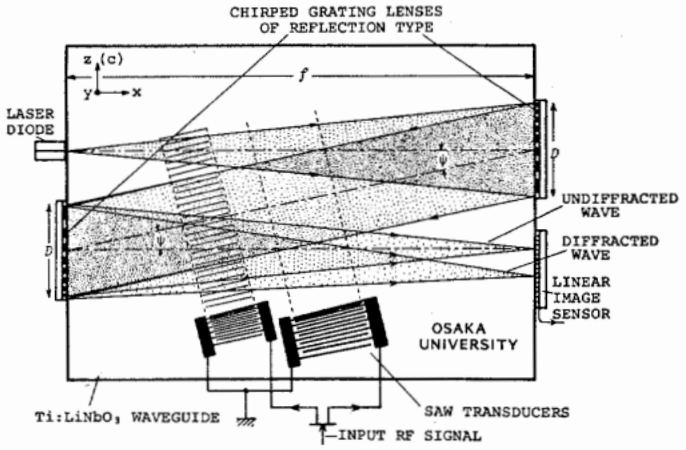

(a)

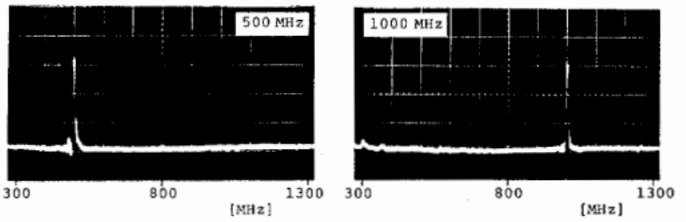

(b)

Fig. 37. A folded-type integrated optic RF spectrum analyzer using butt-coupled chirped grating lenses. (a) Device configuration, (b) output spectrum signal.

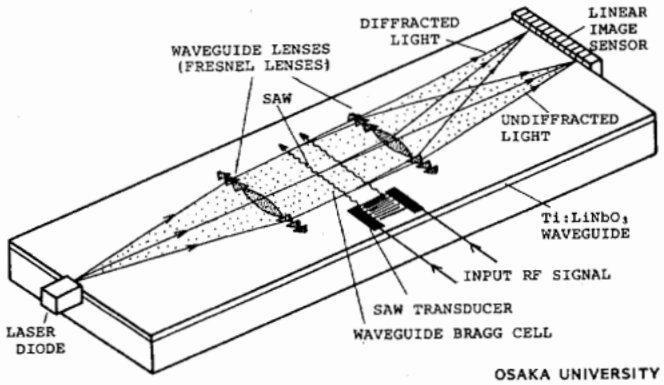

Fig. 38. An integrated optic RF spectrum analyzer using Fresnel lenses.

technique. Another advantage of this IOSA construction is that the use of the off-axis reflection-type CGL's and the resultant folded (z-shaped) optical axis allow a reduced device length. In the device, only the collimated guided wave undergoes the AO interaction with the SAW; the diverging and converging waves have no interaction since they are far from the Bragg condition. To obtain wide-band operation, a two-stage array of tilted-finger chirped IDT's fabricated by the direct EB lithography was adopted. Fig. 37 (b) shows the output spectrum signal obtained with the fabricated device of 15 mm device length; 4 MHz resolution and 1 GHz bandwidth have been achieved. Fig. 38 shows an IOSA using proton-exchanged Fresnel lenses [46]. The device has the advantage that the lenses can be fabricated directly in the $LiNbO_3$ waveguide. In the fabricated devices of 40 mm device length, 1 GHz bandwidth, and 2 and 3 MHz resolutions with an He–Ne laser and laser diode, respectively, have been obtained.

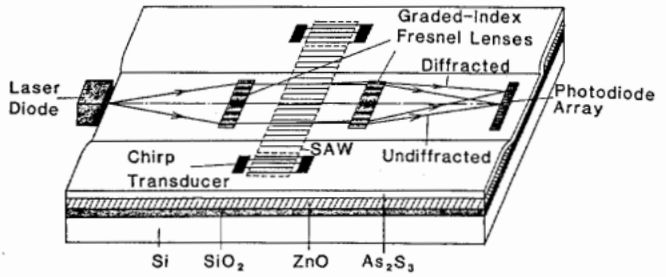

Fig. 39. A monolithic integrated optic Fourier processor using an Si substrate [62].

The frequency resolution of an IOSA is determined by the diffraction-limited focal spot size and the pitch of the available detector array; the former can be as small as 2–3 μm, while the latter is around 10 μm at minimum. Therefore, some interface element would be required in the full integration to match the dimensions without enlarging the IOSA and avoiding the reduction in overall resolution. The use of a fan-out channel guide array shown in Fig. 25 as a focal-plane expander (focal-plane dissector) has been discussed [58].

Another possible IOSA construction is to use focusing grating couplers instead of the waveguide lenses as will be shown in Fig. 41. Then the light beam, after diffraction by the FGC, propagates and is focused in the bulk substrate crystal or in free space. This makes it easy to couple the photodetector array directly with an FGC of long focal length, eliminates the waveguide output-edge defect problem, and makes the device performance less sensitive to possible optical damage. Therefore, the configuration would lead to easy fabrication and assembling and improvements in resolution and dynamic range.

With the achieved full integrating and the performances described above, the fabrication of the $LiNbO_3$-based IOSA's for practical application has come to within or near the present technology. It should be mentioned that, although the above-described IOSA's employ the AO effect, there is another possibility of using the EO effect to perform a discrete spectrum analysis [91]; a lensless IOSA using an EO spatial light modulator has also been proposed and the fundamental operation has been demonstrated [92], [93].

2) Monolilthic Integration Using Si Substrate: The photodetectors and the readout electronics required in IOSA's are desired to be integrated with the optical components on the same substrate. In this integration point of view, it is more attractive to use a Si substrate than a $LiNbO_3$ waveguide. Earlier IOSA developments aimed at the implementation of an IOSA by integrating a Bragg cell and Luneburg lenses in a $Ta_2O_5/SiO_2/Si$ waveguide [94]. In recent years, prototype devices have been fabricated by employing diffraction waveguide lenses.

Fig. 39 shows a schematic illustration of an integrated optic Fourier processor using an acoustooptic Bragg cell and Fresnel lenses in an $As_2S_3/SiO_2/Si$ waveguide [62]. The AO Bragg cell using an amorphous As_2S_3 waveguide

can be highly efficient and of low drive power since the AO figure of merit of As_2S_3 is very large. The Fourier processor can be constructed by integrating a pair of Fresnel lenses. For the SAW excitation in the Bragg cell, ZnO thin-film transducers of uniform and/or chirped periods were integrated. Prototype devices without the photodetectors have been fabricated and the spectrum analyzer function has been examined by using an external detector. The AO Bragg cell exhibited a small-signal sensitivity of 1.2 percent/mW, and a high efficiency of 93 percent was obtained at 230 mW input RF power. An RF frequency bandwidth of nearly one octave (90–170 MHz) has been obtained with chirped SAW transducer.

An IOSA using an $Si_3N_4/SiO_2/Si$ waveguide has been proposed and fabricated [95]. The lenses are GRTH Fresnel lenses fabricated by patterning the SiO_2 overlay cladding by photolithography. A grating coupler and a periodic channel waveguide array are integrated for the input coupling and the output focal-plane-to-detector interface, respectively. A four-stage multiple tilted array SAW transducer using ZnO thin film is adopted to cover a 250 MHz bandwidth centered at 270 MHz. A spectrum analyzer resolution of 6 MHz has been demonstrated.

Although the fundamental spectrum analyzer operations have been demonstrated with Si-based devices, the performances obtained so far are not enough for practical applications. Further examination of the AO deflection at higher frequency is required to know the ultimate performance in this type of device. Although it seems to be rather difficult to achieve a very wide bandwidth with a Si substrate, there is a possibility of the monolithic integration of all the optical and electronic components except for the laser diode source.

D. Correlators and Convolvers

RF signal processing by real-time convolution and correlation is an important and effective technique for improving the signal-to-noise ratio in radar and telecommunication systems. These processes can be performed by acoustooptic interaction [60]; the devices can be implemented by integrating AO Bragg cells and waveguide lenses.

In the AO space-integrating devices, two signals are fed into two cascaded Bragg cells to be converted into spatial signals, and the product is spatially integrated by a lens onto a photodetector to give the output signal. Application of the reference signal with and without time inversions results in correlation and convolution outputs, respectively. In the AO time-integrating correlator, the LD is intensity modulated by a signal and a reference signal is fed into a Bragg cell. The diffracted light is then imaged onto a photodetector array; the correlation signal is read out after integration by the time constant of the detector circuit. The necessary separation of the signal from the background undiffracted light can be realized by inserting a spatial filter between the Fourier transform and reimaging lenses or by making use of anisotropic AO Bragg diffraction [96]. A time–bandwidth product, which is equal to the improvement of SNR, larger than 10^5 is feasible in a time-integrating correlator [60].

A digital correlator employing an EO (electrooptic) grating spatial light modulator and an AO Bragg cell have also been fabricated [97]. The correlation signal between the parallel digital signal applied the EO modulator and the pulse signal fed to the AO Bragg cell is obtained at the photodetector array. The correlation operation of 32 bits digital signal has been demonstrated with external lenses.

Almost all of the elements required to realize integrated optic devices of the above-described RF signal processing of Fourier transform type are included in an IOSA; the technology is a direct extension of the IOSA technique, although the performance requirements for each component become more stringent with the increasing number of components to be integrated. The use of various diffraction lenses could be made to implement many integrated optic RF processing devices.

E. Integrated Optic Disk Pickup Devices

There has been much research and development interest in optical disk memory systems because of the high memory density and capacity and the many applications. Whereas the disk pickup heads are currently constructed with microoptics, implementation by integrated optics using a waveguide would lead to great improvements in producibility, reduction of size, weight, cost, and enhancement of application flexibility. Research has been aimed at the application of focusing grating couplers to such an integrated optic approach. Most recently, a monolithic integrated optic disk pickup device (IODPU) capable of detecting readout and focusing/tracking error signals has been proposed and demonstrated [52].

Fig. 40 (a) shows the schematic illustration of the IODPU. The device is constructed by integrating a focusing grating coupler (FGC), a twin grating focusing beam splitter (TGFBS), and photodiodes in a film waveguide on a Si substrate. The guided wave diverging from the LD is focused by the FGC onto a point on a disk. The wave reflected by the disk is collected and coupled back into the waveguide by the FGC. Then the TGFBS divides the reflected wavefront into halves, deflects (beam splitting), and focuses into two detecting points; the complex function of the TGFBS minimizes the number of the components. Thus, the disk signal is read out, and the focusing/tracking error signals are also obtained by simple processing of the photocurrents based upon the Foucault/push–pull methods, respectively.

The prototype device was fabricated in a glass/SiO_2/Si waveguide with an integrated photodiode as shown in Fig. 31 (c). The FGC/TGFBS gratings were fabricated simultaneously in the same Si–N cladding layer. Fig. 40 (b) shows a microphotograph of FGC/TGFBS and Fig. 40 (c) shows the whole device. The dependence of the output photocurrents on the mirror position is plotted in Fig. 40 (d), with the resultant focusing error signal. Although the performance obtained so far is not sufficient for practical

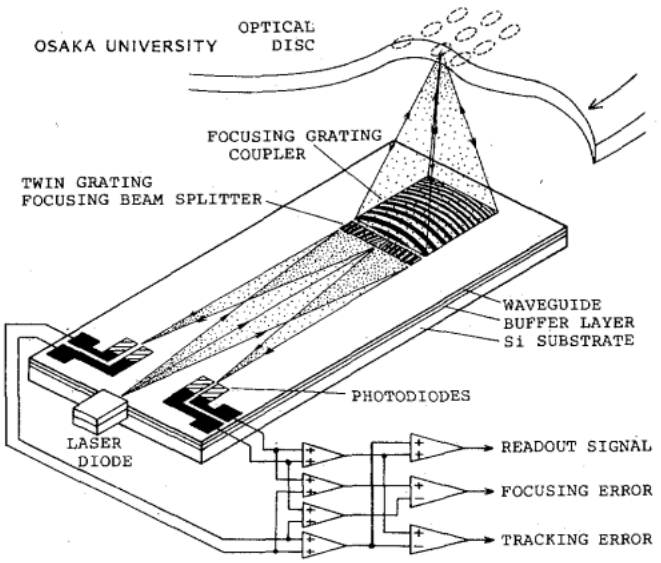

(a)

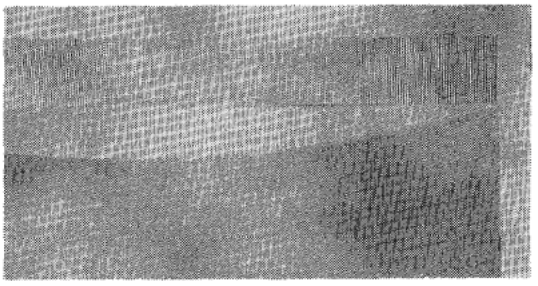

(b)

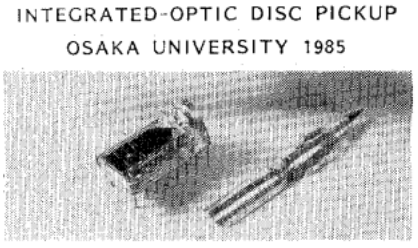

(c)

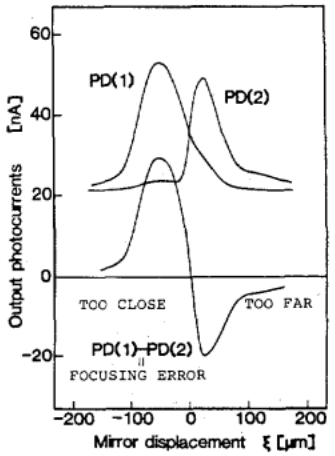

(d)

Fig. 40. An integrated optic disk pickup device. (a) Device construction, (b) microphotograph of FGC/TGFBS gratings, (c) fully integrated device, (d) output signal.

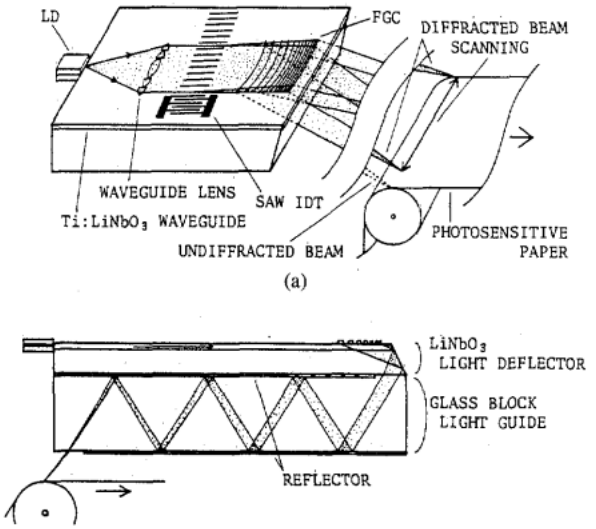

(a)

(b)

Fig. 41. Integrated optic flying spot scanners/printer heads.

application, the fundamental operation, i.e., the detection of readout and focusing/tracking error signals, has been experimentally demonstrated.

F. Integrated Optic Optical Scanners and Printer Heads

Optical scanners are an important element for image processing systems, e.g., optical printers, displays, image readout/conversion devices. Integrated optics could also find applications in this area.

It is evident that an IOSA without a detector serves as a flying spot scanner (FSS) when the Bragg cell is driven by a frequency-sweeping signal. The spot can be magnified and projected onto an image plane by an external lens. The need for a bulky external lens, however, should be eliminated. The important additional requirements for the scanner applications include 1) enlarged focal plane in free space with appropriate working distance, 2) high throughput (low insertion loss), and 3) use of a high-power short-wavelength laser. Integrated optic FSS's satisfying these requirements would evolve from IOSA's.

The above consideration supports the use of focusing grating couplers having a long focal length instead of waveguide lenses. Fig. 41 shows a schematic illustration of an integrated optic flying spot scanner/printer head (IOFSS/IOPH) under development. The possibility of an IOSA using FGC's has been pointed out in Section VI-C1) with the associated advantages. To make the device compact, the output-beam arm can be multiple folded in the glass block, as shown in Fig. 41 (b). The design consideration shows that, with an FGC of 150 mm focal length, 500 resolvable points of 50 μm spot width over a 25 mm long image line are feasible. To generate a pictorial image, the LD or the Bragg cell can be driven with a video signal. In the preliminary experiment, FGC's of substrate radiation type have been fabricated by Si–N and TiO_2 claddings on Ti:$LiNbO_3$ waveguides, and 60 μm spot size and 40 percent efficiency have been obtained with 110 mm focal length [98].

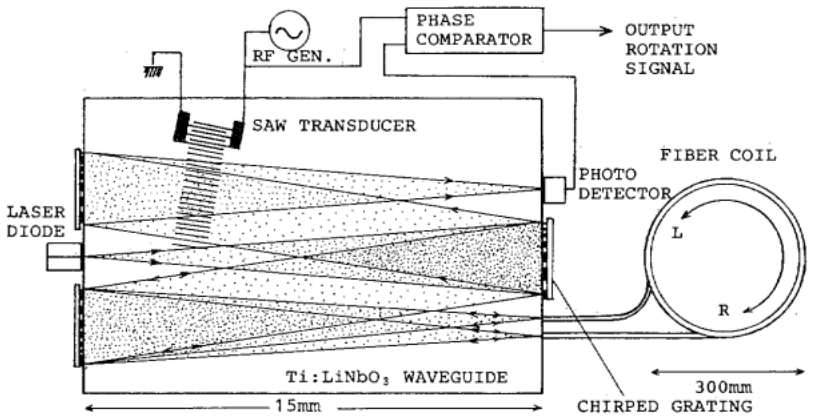

Fig. 42. An integrated optic fiber gyro using grating components.

VII. Future Applications

A. Telecommunication

In the area of optical fiber communication, the work on WDM multi-/demultiplexers and WDM receiver terminals should be continued with dielectric waveguides and extended to devices with semiconductor waveguides. Other applications include the use of grating component as a heterodyne mixer to implement an integrated optic receiver terminal for a coherent transmission system, the use of a chirped grating as a retardation equalizer to enhance the transmission bandwidth, etc. The RF signal-processing devices discussed in Section VI would possibly find applications in spread spectrum telecommunication systems.

B. DFB and DBR Lasers

The most important application of periodic structures in semiconductor lasers and optoelectronic integrated circuits (OEIC's) is distributed feedback (DFB) and distributed Bragg reflection (DBR) structures [4], [11], [12]. Whereas most of the current DFB and DBR lasers are fabricated by holographic interference lithography, applications of EB lithography are also possible [99]. The use of grating components as a beam expander and an output coupler in a semiconductor laser has also been proposed [100]. The EB writing technique, offering higher resolution and larger flexibility, would extend the application in this area, with the improvement in period controllability and the establishment of the optical duplication technique for mass production.

C. Optical Sensors

Sensor applications of integrated optics can be classified into two categories, i.e., 1) processing devices for optical fiber sensors, and 2) integrated optic sensor heads. In both applications, grating elements can be used for input/output interfaces, beam dividing and combining, and wavelength dispersion. An important future work is grating integration to construct interferometers, which are needed in many sensor systems.

In the first category, fiber gyroscopes are currently of great research interest [101]. Integrated coupler optics devices [102] and integrated AO frequency shifters [103], both for fiber gyros, are being developed. An on-wafer gyro using grating components has also been considered [104]. Fig. 42 shows a possible construction of an integrated optic fiber gyro employing the heterodyne detection method. An AO frequency-shifter/beam-combiner and reflection-chirped grating lenses with a beam splitter function are to be integrated. Many alternative configurations exist with the use of other diffraction lenses. Other applications include heterodyne optics devices for fiber laser Doppler velocimeter (LDV), integrated optic multichannel analyzers (evolving from the WDM demultiplexers) for multiwavelength sensing systems, etc.

As a simple example of the second category, a grating coupler for use as a humidity/gas sensor has been reported [105]. An integrated optic position/vibration sensor has been fabricated by integrating an interferometer and a grating coupler for the input–beam interface [106]. A position/vibration sensor can be implemented by modifying the IODPU configuration shown in Fig. 40; a FGC can couple a parallel sensing beam and a DBR grating for the reference beam can be added to construct an interferometer.

D. Optical Computings

There has been growing research interest in digital and analog optical computings [66]. Spectrum analyzers, correlators, and convolvers described in Section VI are examples of specialized optical computing devices. Optical computing systems based upon bulk AO modulators and lenses have been proposed [107]. It is possible to implement integrated optic versions of them by an appropriate combination of grating elements described in Sections IV–VI. An integrated optic device for matrix-vector multiplication using grating components has been proposed and is being developed [108].

E. Optical Interconnections for VLSI Systems

Grating components also will possibly play an important role in the new area of optical interconnection for VLSI systems [109]. The use of a hologram as a routing element has been proposed [109]. In such applications, wavefront conversion gratings (holograms) fabricated by

EB writing in and/or outside waveguiding structures can be used effectively since they do not suffer from the aberration caused by the wavelength discrepancy between fabrication and use.

VIII. Conclusions

Selected research and development topics on integrated optics components and devices using periodic structures have been reviewed. It was demonstrated that the many functions and the integration compatibility of grating components allow implementation of numbers of fully integrated devices incorporating several functions to perform a specific operation. The effective use of electron-beam writing as a versatile microfabrication technique for a variety of grating and periodic components for integration was also demonstrated.

It should be noted that the recent applications are not limited to optical communication, scientific, and industrial purposes, but are extended to office and consumers' uses. Now many applications are within the scope of the present technology. It appears that some of the integrated optic devices reviewed in this paper can be brought to the practical use in the near future, after a short development period, if only the needs are large enough. However, many of them are still of research interest and require further work to improve their performance. It is also hoped that research work in new areas will be activated on the basis of the present technology.

Acknowledgment

The authors wish to thank Prof. J. Koyama for continuous encouragement and support and helpful discussions. They thank their former and present students for their helpful assistance in calculation and experimental work through their thesis work. They also thank to Dr. M. Haruna for helpful discussions.

References

[1] T. Tamir, Ed., *Integrated Optics*. Berlin: Springer-Verlag, 1975.
[2] R. G. Hunsperger, *Integrated Optics: Theory and Technology*. Berlin: Springer-Verlag, 1982.
[3] H. Nishihara, M. Haruna, and T. Suhara, *Optical Integrated Circuits* (in Japanese). Tokyo: Ohm, 1985.
[4] A. Yariv and M. Nakamura, "Periodic structures for integrated optics," *IEEE J. Quantum Electron.*, vol. QE-13, pp. 233–253, 1977.
[5] T. K. Gaylord and M. G. Moharam, "Analysis and applications of optical diffraction by gratings," *Proc. IEEE*, vol. 73, pp. 894–937, 1985.
[6] A. Yariv, "Coupled-mode theory for guided-wave optics," *IEEE J. Quantum Electron.*, vol. QE-9, pp. 919–933, 1973.
[7] See [3, ch. 3 and 4].
[8] H. Kogelnik, "Coupled wave theory for thick hologram gratings," *Bell Syst. Tech. J.*, vol. 48, pp. 2909–2947, 1969.
[9] R. P. Kenan, "Theory of diffraction of guided optical waves by thick holograms," *J. Appl. Phys.*, vol. 46, pp. 4545–4551, 1975.
[10] H. A. Haus and R. V. Schmidt, "Approximate analysis of optical waveguide grating coupling coefficients," *Appl. Opt.*, vol. 15, pp. 774–781, 1976.
[11] H. Kogelnik and C. V. Shank, "Coupled-wave theory of distributed feedback lasers," *J. Appl. Phys.*, vol. 43, pp. 2327–2335, 1972.
[12] S. Wang, "Principles of distributed feedback and distributed Bragg-reflector lasers," *IEEE J. Quantum Electron.*, vol. QE-10, pp. 413–427, 1974.
[13] J. H. Harris, R. K. Winn, and D. G. Dalgoutte, "Theory and design of periodic couplers," *Appl. Opt.*, vol. 11, pp. 2234–2241, 1972.
[14] R. Ulrich, "Efficiency of optical-grating couplers," *J. Opt. Soc. Amer.*, vol. 63, pp. 1419–1431, 1973.
[15] S. T. Peng, T. Tamir, and H. L. Bertoni, "Theory of periodic dielectric waveguides," *IEEE Trans. Microwave Theory Tech.*, vol. MTT-23, pp. 123–133, 1975.
[16] Y. Yamamoto, T. Kamiya, and H. Yanai, "Improved coupled mode analysis of corrugated waveguides and lasers," *IEEE J. Quantum Electron.*, vol. QE-14, pp. 245–258, 1978.
[17] K. Ogawa, W. S. C. Chang, B. L. Sopori, and F. J. Rosenbaum, "A theoretical analysis of etched grating couplers for integrated optics," *IEEE J. Quantum Electron.*, vol. QE-9, pp. 29–42, 1973.
[18] K. Ogawa and W. S. C. Chang, "Analysis of holographic thin film grating coupler," *Appl. Opt.*, vol. 12, pp. 2167–2171, 1973.
[19] T. Tamir and S. Peng, "Analysis and design of grating couplers," *Appl. Phys.*, vol. 14, pp. 235–254, 1977.
[20] R. J. Collier, C. B. Burckhardt, and L. H. Lin, *Optical Holography*. New York: Academic, 1971.
[21] W. W. Ng, C. Hong, and A. Yariv, "Holographic interference lithography for integrated optics," *IEEE Trans. Electron Devices*, vol. ED-25, pp. 1193–1200, 1978.
[22] T. Fujita, H. Nishihara, and J. Koyama, "Blazed gratings and Fresnel lenses fabricated by electron-beam lithography," *Opt. Lett.*, vol. 7, pp. 578–580, 1982.
[23] T. Suhara, H. Nishihara, and J. Koyama, "Electron-beam-induced refractive-index change of amorphous semiconductors," *Japan. J. Appl. Phys.*, vol. 14, pp. 1079–1080, 1975.
[24] H. Nishihara, Y. Handa, T. Suhara, and J. Koyama, "Direct writing of optical gratings using a scanning electron microscope," *Appl. Opt.*, vol. 17, pp. 2342–2345, 1978.
[25] Y. Handa, T. Suhara, H. Nishihara, and J. Koyama, "Scanning-electron-microscope-written gratings in chalcogenide films for optical integrated circuits," *Appl. Opt.*, vol. 18, pp. 248–252, 1979.
[26] ——, "Micrograting for high-efficiency guided-beam deflection fabricated by electron-beam direct writing techniques," *Appl. Opt.*, vol. 19, pp. 2842–2847, 1980.
[27] H. Nishihara, Y. Handa, T. Suhara, and J. Koyama, "Electron-beam directly written micrograting for integrated optical circuits," *Proc. SPIE*, vol. 239, pp. 134–141, 1980.
[28] H. Kotani, M. Kawabe, and S. Namba, "Direct writing of gratings by electron-beam in poly (methyl methacrylate) optical waveguides," *Japan. J. Appl. Phys.*, vol. 18, pp. 279–283, 1979.
[29] T. Suhara, H. Nishihara, and J. Koyama, "The modulation transfer function in the hologram copying process," *Opt. Commun.*, vol. 14, pp. 35–38, 1975.
[30] ——, "Investigation of optimum conditions in hologram copying process" (in Japanese), *Trans. IECEJ*, vol. 59-C, pp. 443–450, 1976.
[31] D. B. Anderson, R. L. Davis, J. T. Boyd, and R. R. August, "Comparison of optical waveguide lens technologies," *IEEE J. Quantum Electron.*, vol. QE-13, pp. 275–282, 1977.
[32] G. Hatakoshi, H. Inoue, K. Naito, S. Umegaki, and S. Tanaka, "Optical waveguide lenses," *Opt. Acta*, vol. 26, pp. 961–968, 1979.
[33] T. Suhara, T. Shiono, H. Nishihara, and J. Koyama, "An integrated-optic spectrum analyzer using grating lenses of reflection type" (in Japanese), Tech. Rep., IECE, Japan, OQE82-26, 1982.
[34] T. Suhara, H. Morita, T. Tanaka, and H. Nishihara, unpublished work, 1984.
[35] G. Hatakoshi and S. Tanaka, "Grating lenses for integrated optics," *Opt. Lett.*, vol. 2, pp. 142–144, 1978.
[36] S. K. Yao and D. E. Thompson, "Chirped-grating lens for guided wave optics," *Appl. Phys. Lett.*, vol. 33, pp. 635–637, 1978.
[37] T. Suhara, H. Nishihara, and J. Koyama, "High-efficiency diffraction-type waveguide lenses fabricated by electron-beam writing," presented at the Topical Meet. Gradient-Index Opt. Imaging Syst., F6, Kobe, Japan, July 4–5, 1983.
[38] S. Forouhar, R. X. Lu, W. S. C. Chang, R. L. Davis, and S. K. Yao, "Chirped grating lenses on Nb_2O_5 transition waveguides," *Appl. Opt.*, vol. 22, pp. 3128–3132, 1983.
[39] S. Forouhar, W. S. C. Chang, and S. K. Yao, "Performance and limitations of chirped grating lenses of Ti-indiffused $LiNbO_3$ planar waveguides," *J. Lightwave Technol.*, vol. LT-2, pp. 503–512, 1984.
[40] C. Warren, S. Forouhar, and W. S. C. Chang, "Double ion exchanged chirp grating lens in lithium niobate waveguides," *Appl. Phys. Lett.*, vol. 43, pp. 424–426, 1983.
[41] W. S. C. Chang and P. R. Ashley, "Fresnel lenses in optical wave-

guides," *IEEE J. Quantum Electron.*, vol. QE-16, pp. 744–753, 1980.
[42] T. Suhara, K. Kobayashi, H. Nishihara, and J. Koyama, "Graded-index Fresnel lenses for integrated optics," *Appl. Opt.*, vol. 21, pp. 1966–1971, 1982.
[43] P. Mottier and S. Valette, "Integrated Fresnel lens on thermally oxidized silicon substrate," *Appl. Opt.*, vol. 20, pp. 1630–1634, 1981.
[44] S. Valette, A. Morque, and P. Mottier, "High-performance integrated Fresnel lenses on oxidized silicon substrate," *Electron. Lett.*, vol. 18, pp. 13–15, 1982.
[45] J. L. Jackel, C. E. Rice, and J. J. Veselka, "Proton exchange for high-index waveguides in $LiNbO_3$," *Appl. Phys. Lett.*, vol. 41, pp. 607–608, 1982.
[46] T. Suhara, S. Fujiwara, and H. Nishihara, "Proton-exchanged Fresnel lenses in Ti : $LiNbO_3$ waveguides," presented at the Topical Meet. Gradient-Index Opt. Imaging Syst., A3, Palermo, Italy, Sept. 26–27, 1985.
[47] J. J. Turner, B. Chen, L. Yang, J. M. Ballantyne, and C. L. Tang, "Gratings for integrated optics fabricated by electron microscope," *Appl. Phys. Lett.*, vol. 23, pp. 333–334, 1973.
[48] J. C. Tracy, L. F. Thompson, R. D. Heidenreich, and J. L. Merz, "Gratings for integrated optics by electron lithography," *Appl. Opt.*, vol. 13, pp. 1695–1702, 1974.
[49] D. G. Dalgoutte, "A high efficiency thin grating coupler for integrated optics," *Opt. Commun.*, vol. 8, pp. 124–127, 1973.
[50] S. T. Peng and T. Tamir, "Directional blazing of waves guided by asymmetrical dielectric gratings," *Opt. Commun.*, vol. 11, pp. 405–409, 1974.
[51] T. Suhara, H. Nishihara, and J. Koyama, "High-performance focusing grating coupler fabricated by electron-beam writing," presented at the Topical Meet. Integrated and Guided-Wave Opt., ThD-4, Kissimmee, FL, Apr. 24–27, 1984.
[52] T. Suhara, S. Ura, H. Nishihara, and J. Koyama, "An integrated-optic disc pickup device," in *Int. Conf. Integrated Opt. and Opt. Fiber Commun., Tech. Dig.*, Venezia, Italy, Oct. 1–4, 1985, pp. 117–120.
[53] T. Suhara, H. Nishihara, and J. Koyama, "Waveguide holograms: A new approach to hologram integration," *Opt. Commun.*, vol. 19, pp. 353–358, 1976.
[54] D. Heitmann and C. Ortiz, "Calculation and experimental verification of two-dimensional focusing grating couplers," *IEEE J. Quantum Electron.*, vol. QE-17, pp. 1257–1263, 1981.
[55] G. Hatakoshi, H. Fujima, and K. Goto, "Waveguide grating lenses for optical couplers," *Appl. Opt.*, vol. 23, pp. 1749–1753, 1984.
[56] S. Somekh, E. Garmire, A. Yariv, H. L. Garvin, and R. G. Hunsperger, "Channel optical waveguide directional couplers," *Appl. Phys. Lett.*, vol. 22, pp. 46–47, 1973.
[57] J. T. Boyd and D. A. Ramey, "Optical channel waveguide arrays coupled to integrated charge-coupled devices and their applications," *Proc. SPIE*, vol. 176, pp. 141–147, 1979.
[58] T. Suhara, M. Morisawa, H. Morita, and H. Nishihara, unpublished work, 1985.
[59] E. G. H. Lean, J. M. White, and C. D. W. Wilkinson, "Thin-film acoustooptic devices," *Proc. IEEE*, vol. 64, pp. 779–788, 1976.
[60] C. S. Tsai, "Guided-wave acoustooptic Bragg modulators for wide-band integrated-optic communications and signal processing," *IEEE Trans. Circuits Syst.*, vol. CAS-26, pp. 1072–1098, 1979.
[61] S. K. Yao, R. R. August, and D. B. Anderson, "Guided-wave acoustooptic interaction on nonpiezoelectric substrates," *J. Appl. Phys.*, vol. 49, pp. 5728–5730, 1978.
[62] T. Suhara, T. Shiono, H. Nishihara, and J. Koyama, "An integrated-optic Fourier processor using an acoustooptic deflector and Fresnel lenses in an As_2S_3 waveguide," *J. Lightwave Technol.*, vol. LT-1, pp. 624–630, 1983.
[63] W. R. Smith, H. M. Gerard, J. H. Collins, T. M. Reeder, and H. J. Shaw, "Design of surface wave delay lines with interdigital transducers," *IEEE Trans. Microwave Theory Tech.*, vol. MTT-17, pp. 865–873, 1969.
[64] T. Suhara, H. Nishihara, and J. Koyama, "One-gigahertz-bandwidth demonstration in integrated-optic spectrum analyzers," presented at the Int. Conf. Integrated Opt. and Optical Fiber Commun., 29c5-5, Tokyo, Japan, June 27–30, 1983.
[65] R. A. Becker and W. S. C. Chang, "Electro optical switching in thin film waveguides for a computer communications bus," *Appl. Opt.*, vol. 18, pp. 3296–3300, 1979.
[66] C. M. Verber, "Integrated-optical approaches to numerical optical processing," *Proc. IEEE*, vol. 72, pp. 942–953, 1984.
[67] J. M. P. Delavaux, G. E. Betts, and W. S. C. Chang, "Electrooptic linear chirped grating lenses on planar optical Ti : $LiNbO_3$ waveguides," *J. Lightwave Technol.*, vol. LT-3, pp. 595–600, 1985.
[68] D. B. Ostrowsky, R. Poirier, L. M. Reibor, and C. Deverdun, "Integrated optical photodetector," *Appl. Phys. Lett.*, vol. 22, pp. 463–464, 1973.
[69] J. D. Spear-Zino, R. R. Rice, J. K. Powers, D. A. Bryan, D. G. Hall, E. A. Dalke, and W. R. Reed, "Multiwavelength monolithic integrated fiber optics terminal: An update," *Proc. SPIE*, vol. 239, pp. 293–298, 1980.
[70] P. K. Tien and R. Ulrich, "Theory of prism-film coupler and thin-film light guides," *J. Opt. Soc. Amer.*, vol. 60, pp. 1325–1337.
[71] Y. Handa, T. Suhara, H. Nishihara, and J. Koyama, "Integrated grating circuit for guided-beam multiple division fabricated by electron-beam direct writing," *Opt. Lett.*, vol. 5, pp. 309–311, 1980.
[72] G. Winzer, "Wavelength multiplexing components—A review of single-mode devices and their applications," *J. Lightwave Technol.*, vol. LT-2, pp. 369–378, 1984.
[73] K. Wagatsuma, H. Sakaki, and S. Saito, "Mode conversion and optical filtering of obliquely incident waves in corrugated optical waveguide filters," *IEEE J. Quantum Electron.*, vol. QE-15, pp. 632–637, 1979.
[74] A. C. Lianos, A. Katzier, A. Yariv, and C. S. Hong, "Chirped-grating demultiplexers in dielectric waveguides," *Appl. Phys. Lett.*, vol. 30, pp. 519–521, 1977.
[75] T. Suhara, Y. Handa, H. Nishihara, and J. Koyama, "Monolithic integrated micrograting and photodiodes for wavelength demultiplexing," *Appl. Phys. Lett.*, vol. 40, pp. 120–122, 1982.
[76] G. L. Tangonan, O. G. Ramor, H. R. Friedrich, C. K. Asawa, D. L. Persechini, and L. E. Gorre, "Planar multimode devices for fiber optics," presented at the Int. Conf. Integrated Opt. and Optical Fiber Commun., 21-5, Amsterdam, The Netherlands, Sept. 17–19, 1979.
[77] R. Watanabe and K. Nosu, "Slab waveguide demultiplexer for multimode optical transmission in the 1.0–1.4 μm wavelength region," *Appl. Opt.*, vol. 19, pp. 3588–3590, 1980.
[78] Y. Fujii and J. Minowa, "Optical demultiplexer using a silicon concave diffraction grating," *Appl. Opt.*, vol. 22, pp. 974–978, 1983.
[79] H. W. Yen, H. R. Friedrich, R. J. Morrison, and G. L. Tangonan, "Planar Rowland spectrometer for fiber-optic wavelength demultiplexing," *Opt. Lett.*, vol. 6, pp. 639–641, 1981.
[80] T. Suhara, J. Viljanen, and M. Leppihalme, "Integrated-optic wavelength multi- and demultiplexers using a chirped grating and an ion-exchanged waveguide," *Appl. Opt.*, vol. 21, pp. 2195–2198, 1982.
[81] E. Voges, "Multimode planar devices for wavelength division multiplexing and demultiplexing," presented at the Int. Conf. Integrated Opt. and Optical Fiber Commun., 29A1-5, Tokyo, Japan, June 27–30, 1983.
[82] H. J. Lilienhof, B. Pantschew, and D. Schulz, "Printed geodesic lenses in glass with ion-exchanged film waveguides," *Electron. Lett.*, vol. 18, pp. 344–345, 1982.
[83] J. Viljanen, T. Suhara, and H. Nishihara, "Multimode spherical geodesic lens for integrated optics," presented at the Nat. Conv. Radio Sci. (Finnish National Committee of URSI), B4, Otaniemi, Finland, Oct. 19–20, 1983.
[84] M. K. Barnoski, B. U. Chen, T. R. Joseph, J. Y. Lee, and O. G. Ramer, "Integrated-optic spectrum analyzer," *IEEE Trans. Circuits Syst.*, vol. CAS-26, pp. 1113–1124, 1979.
[85] D. Mergerian, E. C. Malarkey, R. P. Pautienus, J. C. Bradley, G. E. Marx, L. D. Hutcheson, and A. L. Kellner, "Operational integrated optical RF spectrum analyzer," *Appl. Opt.*, vol. 19, pp. 3033–3034, 1980.
[86] M. Kanazawa, T. Atsumi, M. Takami, and T. Ito, "High resolution integrated optic spectrum analyzer," presented at the Int. Conf. Integrated Opt. and Optical Fiber Commun., 30B3-5, Tokyo, Japan, June 27–30, 1983.
[87] D. Mergerian, E. C. Malarkey, and R. P. Partienus, "High dynamic range integrated optical RF spectrum analyzer," presented at the Int. Conf. Integrated Opt. and Optical Fiber Commun., 30B3-6, Tokyo, Japan, June 27–30, 1983.
[88] R. L. Davis and F. S. Hickernell, "An IO spectrum analyzer with thin film lenses," presented at the Int. Conf. Integrated Opt. and Optical Fiber Commun., WE-6, San Francisco, CA, Apr. 27–29, 1981.
[89] V. Neuman, C. W. Pitt, and L. M. Walpita, "An integrated acoustooptic spectrum analyzer using grating components," in *Proc.*

European Conf. Integrated Opt., London, England, Sept. 14–15, 1981, pp. 89–92.
[90] T. Suhara, H. Nishihara, and J. Koyama, "A folded-type integrated-optic spectrum analyzer using butt-coupled chirped grating lenses," *IEEE J. Quantum Electron.*, vol. QE-18, pp. 1057–1059, 1982.
[91] G. Arvidsson and L. Thylen, "Electrooptic integrated optics spectrum analyzer: An experimental investigation," *Appl. Opt.*, vol. 21, pp. 797–803, 1982.
[92] L. Thylen and L. Stensland, "Lensless integrated optics spectrum analyzer," *IEEE J. Quantum Electron.*, vol. QE-18, pp. 381–385, 1982.
[93] G. Arvidsson and L. Thylen, "Lensless integrated optic spectrum analyzer—An experimental feasibility demonstration," presented at the Int. Conf. Integrated Opt. and Optical Fiber Commun., 30B3-8, Tokyo, Japan, June 27–30, 1983.
[94] D. B. Anderson, J. T. Boyd, M. C. Hamilton, and R. R. August, "An integrated-optical approach to the Fourier transform," *IEEE J. Quantum Electron.*, vol. QE-13, pp. 268–275, 1977.
[95] S. Valette, J. Lizet, P. Mottier, J. P. Jadot, S. Renard, A. Fournier, A. M. Grouillet, P. Gidon, and H. Denis, "Integrated optical spectrum analyzer using planar technology on oxidized silicon substrate," *Electron. Lett.*, vol. 19, pp. 883–885, 1983.
[96] K. Y. Liao, C. C. Lee, and C. S. Tsai, "Time-integrating correlator using guided-wave anisotropic acoustooptic Bragg diffraction and hybrid integration," presented at the Topical Meet. Integrated and Guided-Wave Opt., WA-4, CA, Jan. 6–8, 1982.
[97] C. M. Verber, R. P. Kenan, and J. R. Busch, "Correlator based on an integrated optical spatial light modulator," *Appl. Opt.*, vol. 20, pp. 1626–1629, 1981.
[98] N. Nozaki, T. Suhara, and H. Nishihara, "Focusing grating couplers of long focal length fabricated in Ti : $LiNbO_3$ waveguides" (in Japanese), presented at the Ann. Meet. Japan. Soc. Appl. Phys., 2p-L-12, Kyoto, Japan, Oct. 1–4, 1985.
[99] H. Temkin, G. J. Dolan, N. A. Olsson, C. H. Henry, R. A. Logan, R. F. Kazarinov, and L. F. Johnson, "1.55-μm InGaAsP ridge waveguide distributed feedback laser," *Appl. Phys. Lett.*, vol. 45, pp. 1178–1180, 1984.
[100] G. Evans, J. Learly, and J. Wilcox, "Applications of semiconductor lasers in space communications," *Opt. Eng.*, vol. 22, pp. 247–255, 1983.
[101] S. Ezekiel and H. J. Arditty, Ed., *Fiber-Optic Rotation Sensors*. Berlin: Springer-Verlag, 1982.
[102] H. J. Arditty, J. P. Bettini, Y. Bourbin, P. Graindorge, H. C. Lefevre, M. Papuchon, and S. Vatoux, "Integrated-optic fiber gyroscope: Progresses towards a tactical application," in *Proc. Int. Conf. Opt. Fiber Sensors*, Stuttgart, Germany, Sept. 5–7, 1984, pp. 321–325.
[103] N. Ohgi, M. Kondoh, and M. Shimizu, "Optical fiber gyroscope with integrated optical frequency modulation," in *Proc. Int. Conf. Opt. Fiber Sensors*, Stuttgart, Germany, Sept. 5–7, 1984, pp. 297–300.
[104] S. K. Yao, "Guided-wave optical interferometer using periodic structures," *Proc. SPIE*, vol. 239, pp. 104–109, 1980.
[105] K. Tiefenthaler and W. Lukosz, "Integrated optical switches and gas sensors," *Opt. Lett.*, vol. 9, pp. 137–139, 1984.
[106] P. Gidon, S. Valette, and P. Schweizer, "Vibration sensor using planar integrated interferometric circuit on oxidized silicon substrate," in *Proc. Int. Conf. Opt. Fiber Sensors*, Stuttgart, Germany, Sept. 5–7, 1984, pp. 187–190.
[107] W. T. Rhodes and P. S. Guilfoyle, "Acoustooptic algebraic processing architectures," *Proc. IEEE*, vol. 72, pp. 820–830, 1984.
[108] C. M. Verber, "Integrated optical architectures for matrix multiplication," *Opt. Eng.*, vol. 24, pp. 19–25, 1985.
[109] J. W. Goodman, F. J. Leonberger, S. Kung, and R. A. Athale, "Optical interconnections for VLSI systems," *Proc. IEEE*, vol. 72, pp. 850–866, 1984.

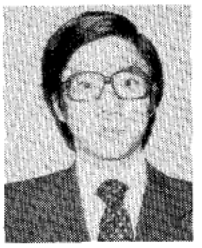

Toshiaki Suhara was born in Wakayama, Japan, on November 13, 1950. He received the B.S., M.S., and Ph.D. degrees in electronics engineering from Osaka University, Osaka, Japan, in 1973, 1975, and 1978, respectively.

He joined the Department of Electronics, Faculty of Engineering, Osaka University, in 1978 as a Research Associate. He is currently engaged in research on integrated optics, optical memories, holography, and applications of electron beams. In 1980 he visited, for three months, the Technical Research Centre of Finland as a Guest Research Scientist.

Dr. Suhara received the Paper Award in 1978 and the Young Engineer Award in 1980, both from the Institute of Electronics and Communication Engineers (IECE) of Japan. He is a coauthor of the volume *Optical Integrated Circuits* (in Japanese). He is a member of the IECE of Japan, the Japan Society of Applied Physics, and the Laser Society of Japan.

Hiroshi Nishihara (S'59–M'68) was born in Osaka, Japan, on August 4, 1937. He received the B.S., M.S., and Ph.D. degrees in communication engineering from Osaka University, Osaka, Japan, in 1960, 1962, and 1965, respectively.

He joined the Department of Electronic Engineering, Faculty of Engineering, Osaka University, and has been a Professor since 1984. His areas of research interest include holography, integrated optics, and optical-fiber sensor techniques.

Dr. Nishihara received the Paper Awards in 1978 and 1983 and the Book Award for *Optical Wave Electronics* in 1980, all from the Institute of Electronics and Communication Engineers (IECE) of Japan, and the Research Award in 1982 from the Laser Society of Japan. He is a member of IECE Japan, the Japan Society of Applied Physics, and SPIE.